Role of quantum fluctuations in a system with strong fields: Spectral properties and Thermalization

Thomas Epelbaum, François Gelis

October 11, 2011

Institut de Physique Théorique (URA 2306 du CNRS)
CEA/DSM/Saclay, 91191 Gif-sur-Yvette Cedex, France

Abstract

In a previous work [arXiv:1009.4363], we have studied the evolution of a scalar field with a quartic coupling, driven by a classical source that initializes it to a non-perturbatively large value. At leading order in the coupling, the evolution of this system is given by classical solutions of the field equation of motion. However, this system is subject to a parametric resonance that leads to secular divergences in higher order corrections to physical observables. We have proposed a scheme that resums all the leading secular terms: this resummation leads to finite results at all times, and we have observed also that it makes the pressure tensor of the system relax to its equilibrium value.

In the present paper, we continue the study of this system by looking at finer details of its dynamics. We first compute its spectral function at various stages of the evolution, and we observe that after a fairly short transient time there are well defined massive quasi-particles. We then consider the time evolution of the momentum distribution of these quasi-particles, and we show that after a stage dominated by the parametric resonance, this distribution slowly evolves to an equilibrium distribution. Interestingly, this distribution develops a transient chemical potential, signalling the fact that number changing processes are much slower than the elastic ones.

1 Introduction

The issue of thermalization is a very challenging question in the theory of heavy ion collisions. On the one hand, a lot of circumstantial evidence suggests that the matter formed in these collisions behaves like a nearly perfect fluid at very short times after the collision (this is based on a comparison of flow measurements with predictions of hydrodynamical models – see [1] for instance). This fact is commonly interpreted as a sign of the fast thermalization of the quark-gluon matter produced in nucleus-nucleus collisions[1]. On the other hand, justifying this thermalization from

[1]Note however than some systems with disordered field configurations may also exhibit an anomalously low viscosity [2, 3].

first principles in QCD has proven to be very difficult, and to this date the question has not been satisfactorily answered.

The main issue is the following: a semi-hard momentum scale –the saturation momentum Q_s– is dynamically generated by the non-linear gluon interactions that occur in nuclear collisions at high energy [4, 5, 6]. This scale controls the so-called gluon saturation phenomenon, that alters the gluonic content of a nucleus at high energy, but it is also this scale that controls the final state interactions that occur after the collision, at least initially. However, the saturation scale Q_s increases with the energy of the collision, and therefore the relevant QCD coupling effectively decreases. It thus seems that the relevant degrees of freedom are rather weakly coupled in collisions at very high energies, rendering difficult the obtention of short thermalization times [7].

To compute the initial gluon production in heavy ion collisions at high energy, we have at our disposal an effective theory –the Color Glass Condensate [8, 9, 10, 11, 12, 13, 14]– that consistently takes into account the non-linear saturation effects. In this effective theory, the degrees of freedom that populate the light-cone wave-function of a nucleus are divided in two classes, according to their longitudinal momentum. Partons with a longitudinal momentum above a certain cutoff Λ are approximated by a collection of static (because they appear highly boosted in the frame of the slower partons) color sources of density $\rho_a(\boldsymbol{x}_\perp)$, while the partons with longitudinal momentum below Λ are treated as standard gauge fields[2] $A^\mu(x)$. In this effective theory, the sources ρ_a are stochastic variables (reflecting the fact that we do not know the precise arrangement of the fast partons at the time of the collision), with a probability distribution $W[\rho]$.

From the above description of the CGC, it may seem that observables could depend on the unphysical cutoff Λ, that has been introduced by hand as a separation scale between the fast and the slow partons. This worry becomes manifest when one computes loop corrections in this framework: they usually contain logarithms of the cutoff Λ. Fortunately, one can show that for sufficiently inclusive observables in the collision of two nuclei, these logarithms are universal in the following sense: (i) they do not depend on the observable under consideration, but are instead properties of the initial state, and (ii) each logarithm of Λ can be assigned to one of the two projectiles (meaning that its coefficient does not depend on the nature of the second projectile). This universality allows to absorb all these logarithms into a redefinition of the distributions $W[\rho]$ of the two projectiles. After this is done, these distributions depend on the cutoff Λ (in such a way as to cancel the Λ dependence that arises from loop corrections), and their changes under variations of the cutoff are controlled by the JIMWLK evolution equation [15, 16, 17, 18, 19, 20, 21, 22, 23, 24, 25].

The Color Glass Condensate, supplemented with the JIMWLK equation, therefore provides a consistent framework for computing observables relevant to heavy ion collisions, such as the spectrum [26, 27, 28, 29, 30, 31, 32] of produced gluons or components of the energy-momentum tensor [33]. However, these computations have also shown that the gluonic matter produced in these collisions is rather far from local equilibrium [34]. In fact, its pressure tensor is highly anisotropic, with two positive transverse pressures and a negative longitudinal pressure. Such a form of the pressure tensor is arguably too far from the equilibrium form to justify the applicability of hydrodynamics (even with viscous corrections).

This computation, a leading order calculation in α_s improved by the resummation of all the leading logarithmic contributions discussed above, is however not the end of the story. It has been noted in various situations [35, 36, 37, 38, 39, 40, 41, 42] that the classical solutions of Yang-

[2] At the leading order of this description, the gluons are dominant over the quarks. Only the former are taken into account in the description.

Mills equations that constitute the LO answer in the CGC approach are unstable under small perturbations. Practically, this means that loop corrections contain secular divergences –i.e. terms that have an unbounded growth with time– and that the perturbative expansion breaks down after a certain time (this time can be estimated to be of the order of Q_s^{-1}, up to logarithms). An additional resummation is therefore necessary in order to circumvent this problem and to obtain expressions that remain well behaved at all times.

Interestingly, the structure of the NLO (1-loop) corrections to inclusive observables in the CGC formalism suggests a natural resummation scheme, that in a loose sense amounts to exponentiating the 1-loop result. Such a resummation first appeared in the context of inflation in cosmology [43, 44]. In the context of the color glass condensate and heavy ion collisions, it was sketched in [45] in the case of gauge fields, and more thoroughly justified[3] in the case of scalar fields in [48]. The reason why a ϕ^4 scalar field theory in four dimensions is an interesting playground for testing these ideas is that this theory, like Yang-Mills theory at the classical level, is scale invariant, and that its classical field configurations are also subject to an instability (due to parametric resonance[4]). The resummation we advocated in [48] can be formulated in two equivalent ways: its derivation leads first to a rather formal expression, in which the resummation is expressed as the action of the exponential of a certain operator on the LO result. This form is not practical for a numerical implementation, but is equivalent to averaging the LO order result (which is expressed in terms of a classical field) over a Gaussian ensemble of initial conditions for the classical field. We then showed that the proposed resummation indeed leads to observables that remain finite at all times, therefore solving the original problem of secular divergences. Moreover, by studying the time evolution of the pressure tensor, we showed that after the resummation, the pressure converges towards its equilibrium value in a fairly short time –something that would not happen with the unresummed expression.

In this paper, we pursue the study of this system of scalar fields, in order to elucidate the microscopic state of the system. In particular, we would like to know whether the system is thermalized when its pressure has relaxed to its equilibrium value, or whether on the contrary one could have an equilibrium-like pressure tensor while the system is still far from equilibrium[5]. A natural quantity to study in order to address this question is the occupation number in the system, and its time evolution. However, even before computing the occupation number, it is interesting to ask whether the system can be described in terms of quasi-particles (this is not trivial: although the system is weakly coupled, it is also very dense, and strong collective effects may render the quasi-particles completely unstable). We start with a reminder of the model and of the main results of [48] in the section 2; then we compute in the section 3 the spectral density of the system, after having justified that it can be resummed in the same way as the energy-momentum tensor. In the section 4, we continue our study with the occupation number. We compute it as a function of momentum up to large times, and identify several stages in its time evolution. In particular, we discuss the possible occurrence of turbulence and Bose-Einstein condensation. From the occupation number, we perform in the section 5 several tests of the quasi-particle picture (e.g. compare the measured

[3]This resummation was also derived in a completely different approach in [46]. The full spectrum of initial fluctuations in Yang-Mills theory in the Fock-Schwinger gauge has been recently derived in [47].

[4]The problem of secular divergences and parametric resonance has been addressed in a number of other approaches in Quantum Field Theory, including perturbation theory (in the regime where the resonant modes are still small) and the 2-Particle Irreducible resummation [49, 50, 51, 52, 53, 54].

[5]In the 2PI approach to the relaxation of a linear sigma model, it has already been observed that an equation of state can be obtained much earlier than the complete thermalization of the system [55].

mass of the quasi-particles, with its value at 1-loop, including medium effects) and compute how the entropy of the system evolves with time. A summary and further discussion can be found in the section 6. In the appendix A, we discuss some aspects of the classical dynamical system to which the quantum field theory is equivalent in our resummation scheme. Some basic properties of the Liouville equation are recalled in the appendix B.

2 Setup of the problem - Summary of previous results

2.1 Model and resummation of secular terms

In [48], we considered a real scalar field theory, with quartic self-interactions, and coupled to an external source. The Lagrangian of this model reads

$$\mathcal{L} \equiv \frac{1}{2}(\partial_\mu\phi)(\partial^\mu\phi) - \underbrace{\frac{g^2}{4!}\phi^4}_{V(\phi)} + J\phi \,. \tag{1}$$

In this model, the source J is nonzero only at negative times, and its purpose is to initialize the fields to a configuration that has a large expectation value at $t = 0$. At positive times, $J = 0$ and the fields evolve by themselves.

In [48], we have studied the time evolution of the energy-momentum tensor of the system. At leading order (tree level) in the coupling g^2, it is simply the energy-momentum tensor of a classical field:

$$\begin{aligned} T^{\mu\nu}_{\rm LO}(x) &= \partial^\mu\varphi\partial^\nu\varphi - g^{\mu\nu}\left[\frac{1}{2}(\partial_\alpha\varphi)^2 - \frac{g^2}{4!}\varphi^4\right], \\ \Box\varphi + \frac{g^2}{3!}\varphi^3 &= J\,, \quad \lim_{x^0\to-\infty}\varphi(x^0,\boldsymbol{x}) = 0\,. \end{aligned} \tag{2}$$

However, at NLO (1 loop) we observed that $T^{\mu\nu}$ is plagued by secular divergences that originate from an instability of the above classical solution, due to parametric resonance. In order to cure this problem, we developed a resummation scheme that collects the leading secular terms at each order of the expansion in g^2. Our resummed expression reads

$$T^{\mu\nu}_{\rm resum}(x) \equiv \exp\Big[\int d^3\boldsymbol{u}\,\beta\cdot\mathbb{T}_{\boldsymbol{u}} + \frac{1}{2}\int d^3\boldsymbol{u}d^3\boldsymbol{v}\int\frac{d^3\boldsymbol{k}}{(2\pi)^3 2k}[a_{+\boldsymbol{k}}\cdot\mathbb{T}_{\boldsymbol{u}}][a_{-\boldsymbol{k}}\cdot\mathbb{T}_{\boldsymbol{v}}]\Big]T^{\mu\nu}_{\rm LO}(x)\,. \tag{3}$$

In this formula, $\mathbb{T}_{\boldsymbol{u}}$ is the generator of shifts of the classical field on the $x^0 = 0$ hypersurface, defined formally by

$$a\cdot\mathbb{T}_{\boldsymbol{u}} \equiv a(0,\boldsymbol{u})\frac{\delta}{\delta\varphi_0(\boldsymbol{u})} + \dot{a}(0,\boldsymbol{u})\frac{\delta}{\delta\dot{\varphi}_0(\boldsymbol{u})}\,, \tag{4}$$

where $\varphi_0(\boldsymbol{u})$ and $\dot{\varphi}_0(\boldsymbol{u})$ are the values of the field and its first time derivative on the surface $x^0 = 0$. This shift operator possesses a very useful property: if $a(x)$ is a small perturbation on top of a classical field $\varphi(x)$, one has

$$a(x) = \int d^3\boldsymbol{u}\,[a\cdot\mathbb{T}_{\boldsymbol{u}}]\,\varphi(x)\,. \tag{5}$$

The fields $a_{\pm \boldsymbol{k}}$ are small perturbations propagating on top of the classical field φ, that are plane waves at $x^0 \to -\infty$, and β is the 1-loop correction to φ,

$$\Big[\Box + V''(\varphi)\Big] a_{\pm \boldsymbol{k}} = 0 \;, \qquad \lim_{x^0 \to -\infty} a_{\pm \boldsymbol{k}}(x) = e^{\pm ik\cdot x} \;,$$
$$\Big[\Box + V''(\varphi)\Big] \beta = -\frac{1}{2} V'''(\varphi) \int \frac{d^3\boldsymbol{k}}{(2\pi)^3 2k}\, a_{-\boldsymbol{k}} a_{+\boldsymbol{k}} \;, \qquad \lim_{x^0 \to -\infty} \beta(x) = 0 \;. \tag{6}$$

(See [48] for more details.) A crucial result is that eq. (3) is equivalent to a functional integration over Gaussian fluctuations of the classical field at $x^0 = 0$,

$$T^{\mu\nu}_{\rm resum} = \int [D\alpha(\boldsymbol{x}) D\dot\alpha(\boldsymbol{x})]\, F[\alpha, \dot\alpha]\; T^{\mu\nu}_{\rm LO}[\varphi_0 + \beta + \alpha] \;, \tag{7}$$

where $T^{\mu\nu}_{\rm LO}[\varphi_0 + \beta + \alpha]$ denotes the LO energy-momentum tensor evaluated with a *classical field* whose initial condition at $x^0 = 0$ is $\varphi_0 + \beta + \alpha$ (and likewise for the first time derivative). The distribution $F[\alpha, \dot\alpha]$ is Gaussian in $\alpha(\boldsymbol{x})$ and $\dot\alpha(\boldsymbol{x})$, with 2-point correlations given by

$$\begin{aligned} \big\langle \alpha(\boldsymbol{x}) \alpha(\boldsymbol{y}) \big\rangle &= \int \frac{d^3\boldsymbol{k}}{(2\pi)^3 2k}\, a_{+\boldsymbol{k}}(0,\boldsymbol{x}) a_{-\boldsymbol{k}}(0,\boldsymbol{y}) \;, \\ \big\langle \dot\alpha(\boldsymbol{x}) \dot\alpha(\boldsymbol{y}) \big\rangle &= \int \frac{d^3\boldsymbol{k}}{(2\pi)^3 2k}\, \dot a_{+\boldsymbol{k}}(0,\boldsymbol{x}) \dot a_{-\boldsymbol{k}}(0,\boldsymbol{y}) \;. \end{aligned} \tag{8}$$

We refer the reader to [48] for more details about the model and its practical lattice implementation.

2.2 Relaxation of the pressure

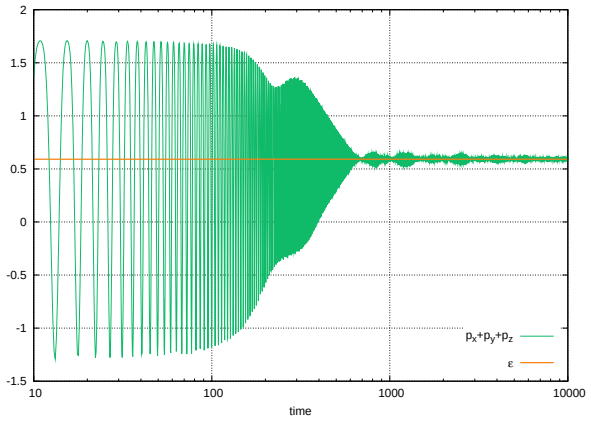

Figure 1: Relaxation of the pressure tensor towards the equilibrium value. All the numerical results presented in this paper have been obtained with a coupling constant $g = 1$.

The main result of [48] is that the fluctuations resummed in the formula (7), in addition to making the resummed quantities free of secular divergences, cause the pressure to relax towards

its equilibrium value (one third of the energy density for a ϕ^4 theory in four dimensions). Without these fluctuations, the pressure is simply that of a classical field configuration, and it oscillates periodically around the equilibrium value, but never relaxes: therefore there is no one-to-one relationship between the pressure and the energy density, and thus no equation of state at LO. The fluctuations of the initial condition for the classical field in eq. (7) produce a decoherence that dampens the oscillations of the pressure, as illustrated in the figure 1, and after a finite time the pressure converges towards the value required by the equilibrium equation of state ($3p = \epsilon$).

In [48], we have also studied the fluctuations of the energy in a small subsystem. Of course, the total energy in the system is conserved and therefore does not fluctuate, but its value in a small subvolume can vary due to exchanges with the surroundings. We have observed a rapid transition from rather narrow Gaussian fluctuations at the starting time to broader fluctuations that are much closer in shape to canonical equilibrium fluctuations at late times. This transition appears to occurs approximately at the same time as the relaxation of the pressure.

2.3 Lattice setup for the study of thermalization

However, the study performed in [48] does not tell us much about the microscopic evolution of the system: indeed, since the energy density and the pressure of the system are intensive quantities that sum over all the modes of the system, the existence of an equation of state identical to the equilibrium one does not imply that the system is in full equilibrium. Equilibrium requires a much more stringent microscopic arrangement of the system, in which the energy is distributed among the various modes in a very specific way. In the present paper, we wish to pursue this study by looking at more microscopic aspects of the system: namely the existence of quasi-particle excitations, and the evolution in time of their momentum distribution. In particular, we would like to know how the energy of the system, initially introduced in the zero mode via a spatially homogeneous external source, eventually goes into higher momentum modes.

A crucial ingredient in this process is the parametric resonance that exists in the ϕ^4 scalar field theory, and therefore it is important that the ultraviolet lattice cutoff be large enough to comprise the resonance band. If the source J is parametrically

$$J \sim \frac{Q^3}{g} \,, \tag{9}$$

then the resonance band is located at momenta of order $k \sim Q$, and the UV cutoff Λ must therefore obey $Q \lesssim \Lambda$. Setting up the lattice cutoff in this way is sufficient to study the evolution of the system at short times, because on these time scales the occupation number remains small above the resonance region, as we shall see later in this paper.

This is however not sufficient if we want to study the approach of the system to thermal equilibrium. In order to see this, recall that the energy density in the system is parametrically

$$\epsilon \sim \frac{Q^4}{g^2} \,. \tag{10}$$

If thermal equilibrium is achieved, this energy density must also be given by the Stefan-Boltzmann formula (at least for reasonably weak couplings),

$$\epsilon \sim T^4 \,, \tag{11}$$

which tells us that the system would equilibrate at a temperature

$$T \sim \frac{Q}{\sqrt{g}} \,. \tag{12}$$

For a numerical simulation to be able to approach the equilibrium state, the lattice ultraviolet cutoff must be large enough to include modes of the order of the temperature, which is a more stringent constraint than simply having the resonance band below the cutoff. At weak coupling, this implies that the resonance band should be located towards the soft sector of the lattice spectrum, i.e. in a region where the lattice mode density is rather low. In order to still have a significant number of lattice modes inside the resonance band, we used a larger lattice (of size 20^3 for the results presented in this paper), and we have chosen the value of the parameter Q so that the resonance band is located near $k \approx 1$ (in lattice units, where the ultraviolet cutoff is at $\Lambda = \sqrt{12}$).

This choice of Q is significantly lower than the value used in [48] (where we were only interested in the early stages of the time evolution, dominated by the resonant modes). This means a lower energy density, and larger time scales. Indeed, since our system is scale invariant, energy density scales like Q^4 and all the times scale like $1/Q$. The resulting time evolution of the pressure, for this choice of Q and a coupling constant $g = 1$, is shown in the figure 1.

3 Spectral function and quasi-particles

3.1 Definition and leading order

Before we study the time evolution of the occupation number in the system, it is interesting to ask an even more elementary question: can the system be described in terms of quasi-particles, or on the contrary does it interact so strongly that no identifiable quasi-particles show up in its spectrum? To that effect, one can compute the spectral function, defined as the imaginary part of the Fourier transform of the retarded propagator[6]:

$$\rho(\omega, \boldsymbol{k}; y^0) \equiv 2\,\mathrm{Im} \int_0^{+\infty} dt d^3\boldsymbol{x}\; e^{i\omega t} e^{-i\boldsymbol{k}\cdot\boldsymbol{x}}\; G_{_R}(y^0 + t, \boldsymbol{x}, y^0, \boldsymbol{0}) \,. \tag{13}$$

In this formula, the retarded propagator is normalized so that

$$\Big[\Box_x + V''(\varphi(x))\Big]\, G_{_R}(x, y) = \delta(x - y) \tag{14}$$

for a classical field configuration φ. A system in equilibrium is invariant under translations in time, and therefore its spectral function defined in this way is in fact independent of the time y^0. However, for transient systems that are not yet in equilibrium, the spectral function will evolve with time and the y^0 dependence is important.

At leading order, we simply need to obtain the retarded propagator in a classical background

[6] We assume here that the system is spatially homogeneous. This is the case in our setup since the source J does not depend on $\boldsymbol{x}$.

field $\varphi(x)$,

$$G_R^{\rm LO}(x,y) = \sum$$ 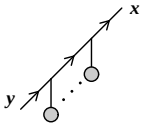

, (15)

where the grey blobs denote the retarded classical field $\varphi(x)$ and the lines with an arrow the bare retarded propagator (the sum is over the number of insertions of the classical field, from 0 to $+\infty$). In a numerical calculation, the simplest way to compute this propagator is to consider a small field perturbation $a(x)$ in that background, that obeys the following equation of motion

$$\Big[\Box_x + V''(\varphi(x))\Big]\, a(x) = 0\,. \tag{16}$$

The fluctuation $a(x)$ can be related to its value at the time y^0 by the following Green's formula

$$a(x) = \int d^3\boldsymbol{y}\, \Big[G_R^{\rm LO}(x,y)\,\big(\partial_y^0 a(y)\big) - \big(\partial_y^0 G_R^{\rm LO}(x,y)\big)\; a(y)\Big]\,, \tag{17}$$

that involves precisely the propagator we are looking for. Thus, by choosing the following initial conditions at time y^0,

$$a(y^0,\boldsymbol{y}) = 0\,, \qquad \partial_y^0 a(y^0,\boldsymbol{y}) = \delta(\boldsymbol{y})\,, \tag{18}$$

the perturbation $a(x)$ is precisely the propagator we need in eq. (13),

$$G_R^{\rm LO}(x^0,\boldsymbol{x},y^0,\boldsymbol{0}) = a(x^0,\boldsymbol{x})\,. \tag{19}$$

Thanks to this observation, we reduce the problem of finding the retarded propagator at leading order to that of solving the equation (16) with the initial conditions of eq. (18), which is easily doable numerically[7].

3.2 Next to leading order and resummation

At next to leading order, three topologies must be evaluated[8]:

$$G_R^{\rm NLO}(x,y) =$$ 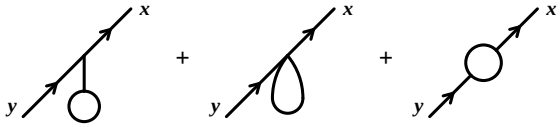

, (20)

where the both the propagators and the vertices are dressed by the classical field $\varphi(x)$. The first topology is the same as the retarded propagator at leading order, in which one of the φ insertions has been replaced by a 1-loop tadpole β defined in eq. (6). Given that this tadpole is given by (see the eq. (39) in [23])

$$\beta(x) = \Big[\int d^3\boldsymbol{u}\;\beta\cdot\mathbb{T}_{\boldsymbol{u}} + \frac{1}{2}\int d^3\boldsymbol{u}d^3\boldsymbol{v}\;\int\frac{d^3\boldsymbol{k}}{(2\pi)^3 2k}[a_{+\boldsymbol{k}}\cdot\mathbb{T}_{\boldsymbol{u}}][a_{-\boldsymbol{k}}\cdot\mathbb{T}_{\boldsymbol{v}}]\Big]\,\varphi(x)\,, \tag{21}$$

[7] On a lattice, the delta function that appears in the initial condition for $\partial_y^0 a(y^0,\boldsymbol{y})$ becomes a Kronecker symbol: the derivative is zero at all points of the lattice except at the origin (0,0,0) where it is equal to one.

[8] Although these diagrams seem to involve cubic vertices, this is not the case. These vertices where three lines merge are in fact proportional to $V'''(\varphi(x))$, and are thus proportional to an extra $\varphi(x)$ that does not appear explicitly in the diagrammatic representation.

it is easy to check that this contribution is related to the leading order one by the following functional identity

$$G_R^{\rm NLO1}(x,y) = \Big[\int d^3\boldsymbol{u}\ \beta\cdot\mathbb{T}_{\boldsymbol{u}} + \frac{1}{2}\int d^3\boldsymbol{u}d^3\boldsymbol{v}\ \int \frac{d^3\boldsymbol{k}}{(2\pi)^3 2k}[a_{+\boldsymbol{k}}\cdot\mathbb{T}_{\boldsymbol{u}}][a_{-\boldsymbol{k}}\cdot\mathbb{T}_{\boldsymbol{v}}]\Big]_{\text{same }\varphi} G_R^{\rm LO}(x,y)\ , \quad (22)$$

where the subscript 'same φ' indicates that the two operators $\mathbb{T}_{\boldsymbol{u}}\mathbb{T}_{\boldsymbol{v}}$ in the second term should act on the same field φ, i.e.

$$\Big[\mathbb{T}_{\boldsymbol{u}}\mathbb{T}_{\boldsymbol{v}}\Big]_{\text{same }\varphi}\varphi(x_1)\cdots\varphi(x_n) \equiv \sum_{i=i}^{n}\varphi(x_1)\cdots\varphi(x_{i-1})\Big[\Big[\mathbb{T}_{\boldsymbol{u}}\mathbb{T}_{\boldsymbol{v}}\Big]\varphi(x_i)\Big]\varphi(x_{i+1})\cdots\varphi(x_n)\ . \quad (23)$$

By using the formula

$$G_{+-}^{\rm LO}(x,y) = \int \frac{d^3\boldsymbol{k}}{(2\pi)^3 2k}\ a_{+\boldsymbol{k}}(x)a_{-\boldsymbol{k}}(y)\ , \quad (24)$$

the second topology can be written as follows,

$$G_R^{\rm NLO2}(x,y) = \Big[\frac{1}{2}\int d^3\boldsymbol{u}d^3\boldsymbol{v}\ \int \frac{d^3\boldsymbol{k}}{(2\pi)^3 2k}[a_{+\boldsymbol{k}}\cdot\mathbb{T}_{\boldsymbol{u}}][a_{-\boldsymbol{k}}\cdot\mathbb{T}_{\boldsymbol{v}}]\Big]_{\text{same }V''(\varphi)} G_R^{\rm LO}(x,y)\ , \quad (25)$$

where the subscript 'same $V''(\varphi)$' indicates that the two operators $\mathbb{T}_{\boldsymbol{u}}\mathbb{T}_{\boldsymbol{v}}$ should act on the same compound $V''(\varphi)$ –one operator on each field of $V''(\varphi)$. The third topology can first be written as

$$G_R^{\rm NLO3}(x,y) = \int d^4w d^4z\ G_R^{\rm LO}(x,w)\Sigma_R^{\rm 1loop}(w,z)G_R^{\rm LO}(z,y)\ , \quad (26)$$

where $\Sigma_R^{\rm 1loop}$ is the 1-loop retarded self-energy,

$$\Sigma_R^{\rm 1loop}(w,z) = \Sigma_{++}^{\rm 1loop}(w,z) - \Sigma_{+-}^{\rm 1loop}(w,z)\ . \quad (27)$$

Next, one can rewrite this self-energy as

$$\Sigma_R^{\rm 1loop}(w,z) = \frac{1}{2}V'''(\varphi(w))V'''(\varphi(z))G_R^{\rm LO}(w,z)\Big[G_{+-}^{\rm LO}(w,z) + G_{-+}^{\rm LO}(w,z)\Big]\ , \quad (28)$$

where the prefactor 1/2 is the symmetry factor of the loop. By combining eqs. (26) and (28) and by using (24), one can finally prove

$$G_R^{\rm NLO3}(x,y) = \Big[\frac{1}{2}\int d^3\boldsymbol{u}d^3\boldsymbol{v}\ \int \frac{d^3\boldsymbol{k}}{(2\pi)^3 2k}[a_{+\boldsymbol{k}}\cdot\mathbb{T}_{\boldsymbol{u}}][a_{-\boldsymbol{k}}\cdot\mathbb{T}_{\boldsymbol{v}}]\Big]_{\text{distinct }\varphi's} G_R^{\rm LO}(x,y)\ , \quad (29)$$

where the qualifier 'distinct φ's' indicates that the two operators $\mathbb{T}_{\boldsymbol{u}}\mathbb{T}_{\boldsymbol{v}}$ must act on two fields φ's that are inserted at different points on the LO propagator $G_R^{\rm LO}$. Adding eqs. (22), (25) and (29) therefore simply lifts any restriction on the action of these operators, and we obtain

$$G_R^{\rm NLO}(x,y) = \Big[\int d^3\boldsymbol{u}\ \beta\cdot\mathbb{T}_{\boldsymbol{u}} + \frac{1}{2}\int d^3\boldsymbol{u}d^3\boldsymbol{v}\ \int \frac{d^3\boldsymbol{k}}{(2\pi)^3 2k}[a_{+\boldsymbol{k}}\cdot\mathbb{T}_{\boldsymbol{u}}][a_{-\boldsymbol{k}}\cdot\mathbb{T}_{\boldsymbol{v}}]\Big] G_R^{\rm LO}(x,y)\ . \quad (30)$$

This formula is formally identical to the formula we have obtained previously for the energy-momentum tensor at NLO, and it leads to the same pathologies due to the presence of secular

divergences. Likewise, the problem can be cured here by performing the same resummation as in the case of the energy-momentum tensor, that amounts to exponentiating the quadratic part of the operator in the square brackets in eq. (30) (as in eq. (3)):

$$G_R^{\text{resummed}}(x,y) \equiv \exp\left[\frac{1}{2}\int d^3\boldsymbol{u}d^3\boldsymbol{v}\int\frac{d^3\boldsymbol{k}}{(2\pi)^3 2k}\,[a_{+\boldsymbol{k}}\cdot\mathbb{T}_{\boldsymbol{u}}][a_{-\boldsymbol{k}}\cdot\mathbb{T}_{\boldsymbol{v}}]\right] G_R^{\text{LO}}(x,y)\,. \tag{31}$$

This resummation amounts to a functional average over Gaussian fluctuations of the initial condition of the classical field at $x^0 = 0$,

$$G_R^{\text{resummed}} = \int\left[D\alpha(\boldsymbol{x})D\dot{\alpha}(\boldsymbol{x})\right]\,F[\alpha,\dot{\alpha}]\,G_R^{\text{LO}}[\varphi_0+\alpha] \tag{32}$$

where the Gaussian distribution $F[\alpha,\dot{\alpha}]$ is defined in eq. (8). Therefore, in order to compute the resummed retarded propagator, we should repeat the procedure outlined in the section 3.1 for every classical field φ obtained from an ensemble of initial conditions $\varphi_0+\alpha$, where α samples the Gaussian distribution $F[\alpha,\dot{\alpha}]$.

3.3 Numerical results

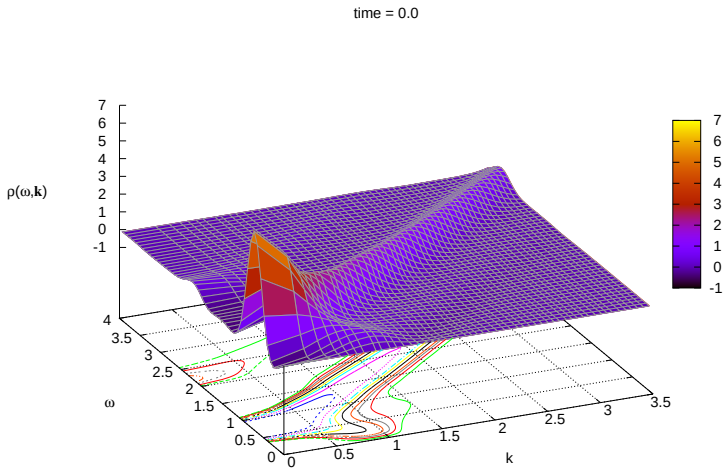

Figure 2: Spectral function $\rho(\omega,\boldsymbol{k};y^0=0.0)$ at the initial time. The computation is done on a 20^3 lattice, for a coupling constant $g=1$. In this plot, k denotes the lattice momentum, i.e. $\sqrt{2(3-\cos(2\pi l/L)-\cos(2\pi m/L)-\cos(2\pi n/L))}$ on a L^3 lattice (l,m,n is the triplet of integers in the range $[0,L-1]$ that labels a given momentum state).

At the initial time (see the figure 2), the spectral function has a fairly complicated structure. Although the large $\boldsymbol{k}$ modes have a single spectral peak at $\omega\approx|\boldsymbol{k}|$, the situation is richer in the soft sector. There, besides the main branch that continues to large $\boldsymbol{k}$, the spectral density exhibits

additional branches. One of them corresponds to a higher mass excitation, and another one has a mass comparable to the main branch but an anomalous dispersion such that the frequency decreases while the momentum increases. Therefore, at early times, the quasi-particle picture is not a good description of the degrees of freedom in the system.

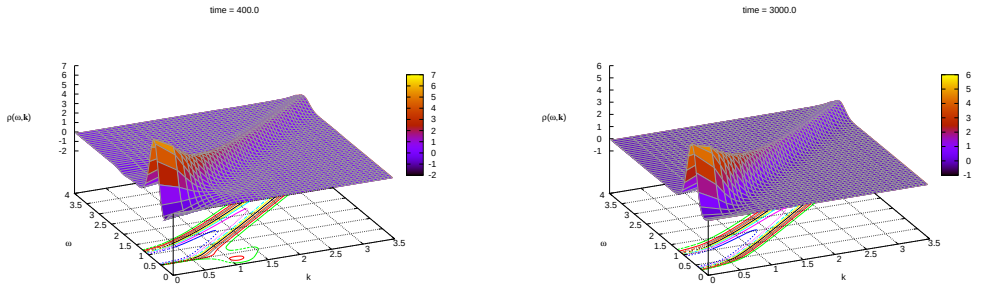

Figure 3: Spectral function $\rho(\omega, \boldsymbol{k}; y^0)$ at the times $y^0 = 400$ (left) and $y^0 = 3000$ (right). The computation is done on a 20^3 lattice, for a coupling constant $g = 1$.

As the time increases, these extra branches in the spectral function decrease in amplitude and eventually disappear, starting with the higher mass excitation. Ultimately, only the main excitation remains, as one can see in the plot on the right of the figure 3 at a time $y^0 = 3000$. At intermediate times (such as $y^0 = 400$, represented on the plot on the left of the figure 3), one gets closer to the spectral function of a system made of quasi-particles, with only small remnants of the structures that existed at early times. It is interesting to note that the characteristic time for the disappearance of the extra branches in $\rho(\omega, \boldsymbol{k}; y^0)$ is comparable to the relaxation time of the pressure, that we have found in the previous section to start at a time of the order of $y^0 \sim 100$.

3.4 Quasi-particle mass

In order to further assess the existence of quasi-particles in the system, one can try to fit the main branch of the spectral function by a function of the form $\omega = \sqrt{\boldsymbol{k}^2 + m^2}$. The result of this fit is shown in the figure 4. One sees that the mass m resulting from this fit is not stable until a time $y^0 \approx 100$, and becomes much more regular afterwards. This is in agreement with the previous qualitative observation that only the main branch of the spectral function survives after this time. Moreover, after $y^0 \geq 1000$, the mass of the quasi-particles that populate the system decreases slowly with time, indicating that the system is not yet completely equilibrated (the change in the mass of the quasi-particles reflects a change in the occupation number of the various modes of the system, that we will study more directly in the following section). If one takes as a crude estimate the Hard Thermal Loop [56, 57] expression of the medium-generated mass (see for instance [58], pp 41–45),

$$m^2_{\text{HTL}} = g^2 \int \frac{d^3\boldsymbol{k}}{(2\pi)^3 2k}\, f_{\boldsymbol{k}} \,, \tag{33}$$

as a function of the occupation number $f_{\boldsymbol{k}}$, we can interpret the decrease of the mass as a shift of the occupation number from low $\boldsymbol{k}$ to higher $\boldsymbol{k}$'s if the total number of quasiparticles ($N \sim \int d^3\boldsymbol{k}\, f_{\boldsymbol{k}}$)

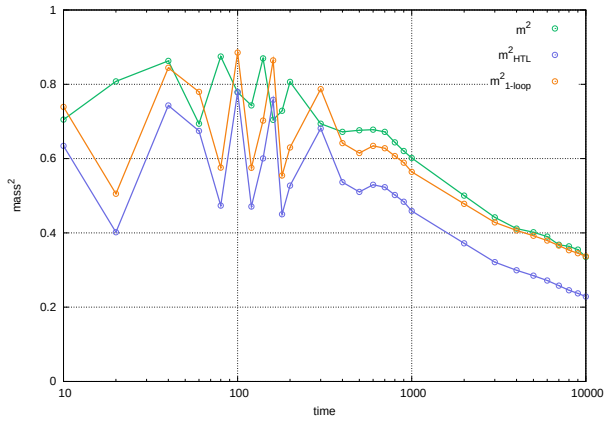

Figure 4: Green line: quasi-particle mass obtained by a fit of the main dispersion branch with a function of the form $\omega = \sqrt{\boldsymbol{k}^2 + m^2}$. Blue line: 1-loop analytic calculation from the occupation number. Red line: 1-loop gap equation that resums recursively all the daisy diagrams. (See the text in section 5 for explanations regarding the curves labelled $m^2_{\rm HTL}$ and $m^2_{1-\rm loop}$.)

is approximately constant.

A word of caution should be added about the width of the quasi-particles. The width of the spectral peak in the figures 2 and 3 is probably not the physical width: for practical reasons the numerical computation of the Fourier transform in time in eq. (13) cannot integrate up to very large times[9]. Thus the width we see in the resulting plots is to a large extent contaminated by the fact that the time interval is finite in the numerical calculation (for the physical width to be visible unambiguously in these plots, the length of the time interval would have to be much larger than the lifetime of the quasi-particles).

4 Occupation number

4.1 Expression in terms of G_{+-} and G_{-+}

Now that we know that at times $x^0 \geq 100$, the spectral content of the system reduces to simple quasi-particles, it makes sense to compute their occupation number. Recall that the creation and annihilation operators $a^\dagger_{\boldsymbol{k}}, a_{\boldsymbol{k}}$ are related to the field operator $\hat\phi$ via

$$\begin{aligned} a_{\boldsymbol{k}} &= i \int d^3\boldsymbol{x}\; e^{ik\cdot x} \overset{\leftrightarrow}{\partial}_{x^0} \hat\phi(x) \\ a^\dagger_{\boldsymbol{k}} &= -i \int d^3\boldsymbol{x}\; e^{-ik\cdot x} \overset{\leftrightarrow}{\partial}_{x^0} \hat\phi(x)\,. \end{aligned} \tag{34}$$

[9] One can check in the free case that this is a very singular Fourier transform. At $\boldsymbol{k} = 0$, it is of the form $\int_0^{+\infty} dt\; t\; \exp(i\omega t) \sim \delta'(\omega)$.

From this, we get the following two reduction formulas

$$\begin{aligned}\left\langle a^\dagger_{\boldsymbol{k}} a_{\boldsymbol{k}} \right\rangle &= \int d^3\boldsymbol{x} d^3\boldsymbol{y}\; e^{ik\cdot(x-y)}\;\overset{\leftrightarrow}{\partial}_{x^0}\overset{\leftrightarrow}{\partial}_{y^0}\; G_{+-}(x,y)|_{x^0=y^0} \\ \left\langle a_{\boldsymbol{k}} a^\dagger_{\boldsymbol{k}} \right\rangle &= \int d^3\boldsymbol{x} d^3\boldsymbol{y}\; e^{ik\cdot(x-y)}\;\overset{\leftrightarrow}{\partial}_{x^0}\overset{\leftrightarrow}{\partial}_{y^0}\; G_{-+}(x,y)|_{x^0=y^0}\;,\end{aligned} \tag{35}$$

with the understanding that the times x^0 and y^0 are set equal only after the derivatives have been evaluated.

It turns out to be more straightforward to calculate the sum of these two expectation values,

$$\left\langle a^\dagger_{\boldsymbol{k}} a_{\boldsymbol{k}} + a_{\boldsymbol{k}} a^\dagger_{\boldsymbol{k}} \right\rangle = \int d^3\boldsymbol{x} d^3\boldsymbol{y}\; e^{ik\cdot(x-y)}\;\overset{\leftrightarrow}{\partial}_{x^0}\overset{\leftrightarrow}{\partial}_{y^0}\; G_s(x,y)|_{x^0=y^0} \tag{36}$$

where $G_s \equiv G_{+-} + G_{-+}$, because in our framework the symmetric propagator G_s is easier to compute than the separate $G_{\pm\mp}$. The occupation number $f_{\boldsymbol{k}}$ is related to the left hand side of eq. (36) by

$$2\omega_{\boldsymbol{k}} V(1+2f_{\boldsymbol{k}}) = \left\langle a^\dagger_{\boldsymbol{k}} a_{\boldsymbol{k}} + a_{\boldsymbol{k}} a^\dagger_{\boldsymbol{k}} \right\rangle\;, \tag{37}$$

where V is the volume of the system and $\omega_{\boldsymbol{k}}$ the dispersion relation of the quasi-particles.

4.2 Calculation of G_s

Let us now see how to compute the symmetric propagator $G_s(x,y)$ at LO, NLO and in the resummation scheme we have developed to cure the pathologies related to secular divergences. At leading order, it is simply given by the product of two classical fields at the points x and y,

$$G_s^{\rm LO}(x,y) = 2\varphi(x)\varphi(y)\;. \tag{38}$$

At next to leading order, G_s is made of two pieces:

i. a 1-loop correction β to one of the factors φ of the LO result,

ii. a connected (tree-level) contribution $\mathcal{G}_s \equiv \mathcal{G}_{+-} + \mathcal{G}_{-+}$ that links the points x and y,

$$G_s^{\rm NLO}(x,y) = 2\Big[\beta(x)\varphi(y) + \varphi(x)\beta(y)\Big] + \mathcal{G}_s(x,y)\;. \tag{39}$$

The second term is given by

$$\mathcal{G}_s(x,y) = \int \frac{d^3\boldsymbol{k}}{(2\pi)^3 2k}\,\Big[a_{+\boldsymbol{k}}(x)a_{-\boldsymbol{k}}(y) + a_{-\boldsymbol{k}}(x)a_{+\boldsymbol{k}}(y)\Big]\;. \tag{40}$$

The $a_{\pm\boldsymbol{k}}$'s can be formally related to the classical field $\varphi(x)$ by (see eq. (5))

$$a_{\pm\boldsymbol{k}}(x) = \int d^3\boldsymbol{u}\;[a_{\pm\boldsymbol{k}}\cdot\mathbb{T}_{\boldsymbol{u}}]\;\varphi(x)\;, \tag{41}$$

while for the tadpole β we can use eq. (21). Then, it is straightforward to combine the two terms to obtain

$$G_s^{\rm NLO}(x,y) = \Big[\int d^3\boldsymbol{u}\;\beta\cdot\mathbb{T}_{\boldsymbol{u}} + \frac{1}{2}\int d^3\boldsymbol{u} d^3\boldsymbol{v}\;\int\frac{d^3\boldsymbol{k}}{(2\pi)^3 2k}[a_{+\boldsymbol{k}}\cdot\mathbb{T}_{\boldsymbol{u}}][a_{-\boldsymbol{k}}\cdot\mathbb{T}_{\boldsymbol{v}}]\Big]\,G_s^{\rm LO}(x,y)\;. \tag{42}$$

From here, it is clear that one can perform the same resummation, where one exponentiates the quadratic part of the operator in the square brackets. This amounts to an average over Gaussian fluctuations of the initial classical field at $x^0 = 0$,

$$G_s^{\text{resummed}}(x,y) = 2\int \left[D\alpha D\dot{\alpha}\right] F[\alpha,\dot{\alpha}] \left[\varphi(x)\varphi(y)\right]_{\varphi_0+\alpha}, \tag{43}$$

where the subscript $\varphi_0 + \alpha$ indicates the initial condition used at $x^0 = 0$ to start the evolution of the classical field φ. $F[\alpha,\dot{\alpha}]$ is the Gaussian distribution of fluctuations defined in eqs. (7) and (8).

4.3 Time evolution of $f_{\boldsymbol{k}}$

By combining the previous results, the occupation number obtained in this resummation scheme can be written as

$$f_{\boldsymbol{k}} = -\frac{1}{2} + \frac{1}{2\omega_{\boldsymbol{k}} V}\int \left[D\alpha D\dot{\alpha}\right] F[\alpha,\dot{\alpha}] \left|\int d^3\boldsymbol{x}\; e^{i\boldsymbol{k}\cdot\boldsymbol{x}} \left(\dot{\varphi}(x^0,\boldsymbol{x}) + i\omega_{\boldsymbol{k}}\varphi(x^0,\boldsymbol{x})\right)\right|^2_{\varphi_0+\alpha}. \tag{44}$$

In the evaluation of this formula, we use for the energy $\omega_{\boldsymbol{k}} = \sqrt{\boldsymbol{k}^2 + m^2}$ with the mass fitted in the previous section (thus, we use a different mass at each time x^0). The result of this calculation

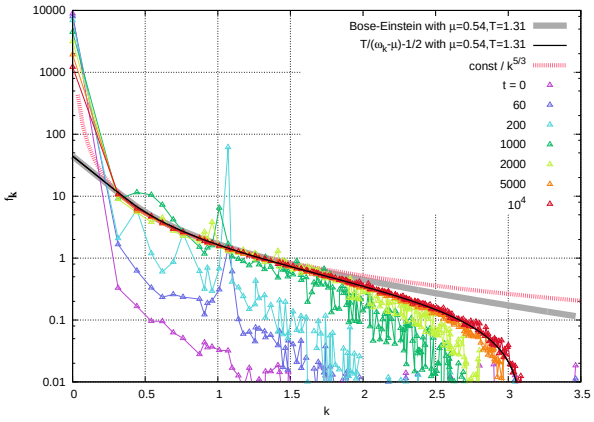

Figure 5: Occupation number $f_{\boldsymbol{k}}$ at various times in the evolution of the system. The grey band represents a fit by a Bose-Einstein distribution. The dashed red band is a fit by a pure power law $k^{-5/3}$. The thin black line is a fit by a distribution of the form given in eq. (46).

is displayed in the figure 5, where we show the occupation number at various stages of the time evolution, as well as three fits that we shall discuss shortly.

Let us first briefly describe the main stages of the time evolution. At the initial time $t = 0$, only the zero mode is occupied and the higher modes have a negligible occupation number. This is a direct consequence of our setup, where the classical field is initially driven by a spatially homogeneous source. Then, shortly afterwards (this is already visible in the spectrum at $t = 20$) one sees an increase of the occupation in the non-zero modes, concomitant with a decrease of the

occupation in the zero mode (barely visible in the figure, due to the logarithmic vertical scale). The increase of the non-zero modes is most pronounced in a narrow band of k, where it peaks more than an order of magnitude above the rest of the curve. One can check[10] that this band of k coincides with the band of parametric resonance that we have discussed in detail in [48]. Thus, it appears that the dominant physics at early times is that of resonance, which leads to a quick increase of the occupation number in a narrow region of $\boldsymbol{k}$. After $t = 1000$, the resonance peak has disappeared and the evolution becomes fairly slow.

Let us now discuss fits of the occupation number, that are represented in the figure 5. The first two are a fit by a Bose-Einstein distribution,

$$f_{\rm BE}(k) = \frac{1}{e^{\beta(\omega_{\boldsymbol{k}}-\mu)} - 1} \,, \tag{45}$$

and a fit by a classical distribution of the form

$$f_{\rm class}(k) = \frac{T}{\omega_{\boldsymbol{k}} - \mu} - \frac{1}{2} \,. \tag{46}$$

Interestingly, the best fit we could achieve with a Bose-Einstein distribution required a non-zero chemical potential. Although the particle number has no reason to be conserved in this theory (there is no symmetry protecting it), this suggests that changes of the particle number are slow compared to the evolution of the distribution in momentum space: a chemical potential at the latest times we have considered indicates that the particle number has not yet reached its equilibrium value (and its positive sign means that we have a particle excess). At weak coupling, this is rather

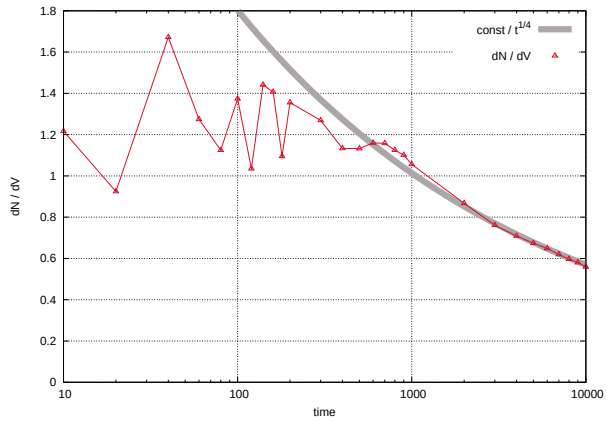

Figure 6: Time evolution of the quasi-particle density in the system. Gray band: fit of the tail with a power law $t^{-1/4}$.

natural: inelastic processes have a much smaller rate than the elastic ones[11], and therefore at

[10] See the appendix B of [48].

[11] For the ϕ^4 scalar theory that we consider here, $\sigma_{\rm el} \sim g^4$, while $\sigma_{\rm inel} \sim g^8$. The hierarchy between the elastic and inelastic time-scales is certainly less pronounced in QCD (see [59]) and there it is unclear whether there is enough time for the formation of a transient state that has a non-zero chemical potential.

intermediate time scales the number of particles is an approximately conserved quantity. In order to check this hypothesis, we can evaluate the number density by summing the occupation number over all the modes $\boldsymbol{k}$. This has been done in the figure 6. One sees indeed that, after a period of somewhat erratic evolution (that roughly corresponds to the time necessary to have well defined quasi-particles in the system), the number density decreases very slowly at late times, as a small negative power of time.

It is also obvious from the figure 5 that a Bose-Einstein distribution does not fit well the occupation number in the tail at large k. In fact, the contrary would have been surprising, since our computation is essentially semi-classical. Naively, one may expect to obtain a classical distribution of the form $T/(\omega_{\boldsymbol{k}} - \mu)$ (again, a non-zero μ is allowed if number changing processes are very slow), but one can check that such a distribution does not produce a better fit of the tail. At first sight, one could be tempted to blame this drop in the tail on the rarefaction of the lattice modes at large k (see for instance the figure 15 in [48]). However, this assumption does not hold if one does the same simulation with lower physical scales, as is done in the figure 7. On this figure, one sees the same drop, now occurring at a smaller value of k. If the drop was caused by lattice artifacts, one would expect it to occur at a fixed value of k (in lattice units), no matter what the physical scales are.

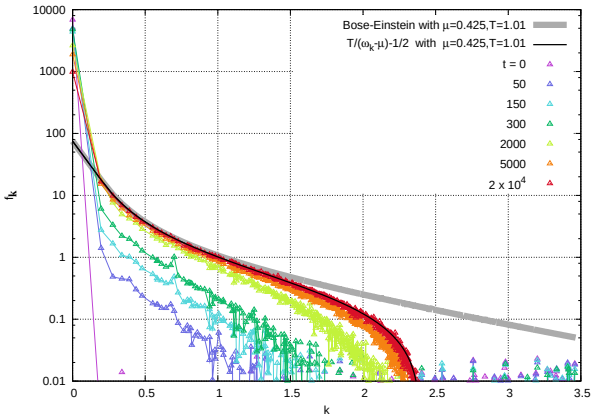

Figure 7: Occupation number $f_{\boldsymbol{k}}$ at various times in the evolution of the system, for a system initialized with a smaller energy density.

It turns out that this drop has a rather trivial explanation. Firstly, note that a very good fit is obtained with the distribution given in eq. (46) (the thin black line in the figures 5 and 7), that differs from the naive classical distribution by an extra $-1/2$ term. This extra term, that makes the fit considerably better, has a simple origin: it comes from the $-1/2$ in the equation (44), which in the derivation of the formula for $f_{\boldsymbol{k}}$ can be traced back to the non-zero commutator between creation and annihilation operators. Keeping this $-1/2$ correction in the definition of the occupation number for a semi-classical calculation is to a large extent an arbitrary choice. Indeed, such an approximation is expected to reproduce correctly the underlying quantum theory only in the region where the occupation number is sufficiently large. When this is the case, one has $f_{\boldsymbol{k}} + 1/2 \approx f_{\boldsymbol{k}}$, and therefore this $1/2$ is not very significant. This also means that the drop of

the occupation number at $k \geq 2$ in the figure 5, although perfectly understandable in our semi-classical approximation, is obviously not a physical feature of the underlying quantum theory[12]. In our setup, there is one advantage in keeping the $-1/2$ in eq. (44) though: if one does the same computation with a vanishing source $J = 0$, one gets identically $f_{\boldsymbol{k}} = 0$, which is of course the exact answer. Without this $-1/2$, one would have obtained $f_{\boldsymbol{k}} = 1/2$.

4.4 Kolmogorov turbulence

At $t \approx 200$, the modes in the resonance band reach their maximal occupancy, and start to subside afterwards, while the other non-zero modes continue to increase. While the resonance peak progressively disappears, one sees in the figure 5 that the occupation curves tend to accumulate in the intermediate k range on a fixed line that is well fitted by a power law $k^{-5/3}$. In this regime, the zero mode continues to decrease, while the occupation curve extends slowly into the hard region.

Such a scaling with an exponent $-5/3$ in the power law is well know in the physics of turbulence (see the first part of [62] for instance). Typically, in Kolmogorov's turbulence, the energy cascades to the hard modes from a source localized in the soft sector, with an intermediate stationary distribution in between, that follows a power law $k^{-5/3}$. In our case, the zero mode plays the role of this source, since it was initially the only occupied mode. In contrast to the usual setup in the study of Kolmogorov's turbulence [62], our system is closed and eventually the zero mode will run out of energy and will not be able to feed the cascade anymore. However, in our simulation, we have not reached the time at which this starts to happen.

4.5 Bose-Einstein condensation

In the figure 5, we saw that the occupation number at late times is best fitted by a distribution of the form of eq. (46). This fit however calls for two comments:

- **i.** the occupation number of the zero mode lies above the curve provided by this fit,
- **ii.** the best value of the chemical potential ($\mu = 0.54$) is close to the mass of the quasi-particles at this time, $m = 0.58$.

These two seemingly unrelated facts have a common interpretation. As we have seen before, a chemical potential arises because the number of quasi-particles evolves very slowly in this system, and a positive μ is the reaction of the system to accommodate an excess of particles. However, it is clear from eqs. (45) and (46) that μ cannot be larger than the mass m – otherwise, the occupation number would become negative near $k = 0$. But having an upper bound on the chemical potential implies an upper bound on the particle density that these distributions can describe. What if the particle excess in the system is so large that the density is larger than this upper bound? When this happens, the excess of particles condenses on the zero mode, a phenomenon known as Bose-Einstein condensation. Dynamically, the system evolves towards a distribution made of two

[12] Interestingly however, the $-1/2$ term in eq. (46) is nothing but the second term in the expansion of the Bose-Einstein distribution in powers of $(\omega_{\boldsymbol{k}} - \mu)/T$. Therefore, at a formal level, keeping this 1/2 correction in the present semi-classical computation gives a better approximation of the full quantum theory. This point was already discussed extensively in [60, 61] in the context of the Boltzmann equation.

components[13],

$$f_{\boldsymbol{k}} = \frac{1}{e^{\beta(\omega_{\boldsymbol{k}}-m)}-1} + f_0\,\delta(\boldsymbol{k})\ , \tag{47}$$

i.e. the chemical potential settles to the maximal value $\mu = m$, and the extra particles go into the zero mode[14] $\boldsymbol{k} = 0$. As one can see from the fit of the figure 5, the occupation number at low $\boldsymbol{k}$ appears to be precisely of the form of eq. (47).

From the knowledge of the occupation number, it is easy to compute what fraction of the number of particles and what fraction of the total energy are contained in the zero mode at various times. This information is provided in the two plots of the figure 8. At early times (up to $t \sim 100$),

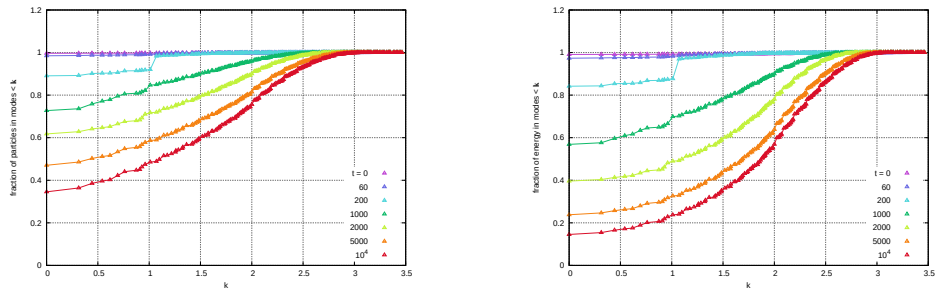

Figure 8: Left: fraction of particles contained in the modes $|\boldsymbol{l}| \leq |\boldsymbol{k}|$, at various stages of the time evolution. Right: fraction of energy contained in the modes $|\boldsymbol{l}| \leq |\boldsymbol{k}|$.

all the particles and all the energy are stored in the zero mode, as a consequence of our initial condition. At intermediate times (e.g. at $t = 200$), a large fraction of the energy is still in the zero mode, and the remainder is almost entirely in the resonance band. At the latest time we have considered ($x^0 = 10^4$ lattice units), the zero mode still contains about 35% of the particles and 15% of the energy.

On could argue that our computation does not demonstrate Bose-Einstein condensation, because we started from an initial condition in which all the energy is already stored in the zero mode. What if we had started from a situation where the zero mode is empty? We have done that in the figure 9, in which the energy of the system is initially contained in the modes[15] $(k_x, k_y, k_z) = (1, 1, 0)$ and $(-1, -1, 0)$ (the total energy being exactly the same as in the figure 5). Thus, at the initial time, the occupation number has a delta peak at a single, non-zero, energy. But then, one sees that a non-zero occupation number develops in the zero mode (and in other modes as well), to reach very large values in a rather short time. After this rapid transient regime, all trace of the original peak has been washed out. At late times, the distribution has become identical to the one encountered in the figure 5: all the modes except $\boldsymbol{k} = 0$ are described by a function of the form of eq. (46), and there is a particle excess in the zero mode. This study strongly suggests that

[13] Here we have written the quantum version of the distribution, but it has an analogue in our semi-classical approximation, where the first term is replaced by $f_{\rm class}(\boldsymbol{k})$. This is discussed in more detail in the appendix A.

[14] Using the Boltzmann equation, it is easy to see that $\boldsymbol{k} = 0$ is the only mode where the extra particles can go. If the particles in excess occupy non-zero modes, then one does not have a fixed point of the Boltzmann equation.

[15] We initialize the system in two opposite modes so that there is no net momentum in the system.

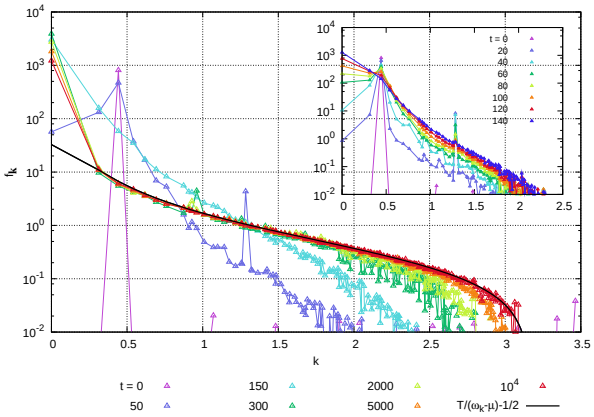

Figure 9: Occupation number $f_{\boldsymbol{k}}$ at various times, for a system initialized in the modes $(k_x, k_y, k_z) = (1, 1, 0)$ and $(-1, -1, 0)$. In the top right inset, we show the behavior at short times.

Bose-Einstein condensation indeed occurs in this system[16], when it is initially over-occupied.

5 Further tests of the quasi-particle description

5.1 Quasi-particle mass

From the occupation number, we can further test the quasi-particle description of the system. A simple check is to compute the medium-induced mass of the quasi-particles, assuming that perturbation theory applies. The Hard Thermal Loop contribution to this mass has already been given in eq. (33), and we have represented this quantity in the figure 4 (blue curve), along with the mass obtained by fitting the location of the peak in the spectral function. In the region where quasi-particles are well defined ($y^0 \geq 100$), we see that the HTL value of the mass is systematically lower than the observed one. We can improve this result by including also the 1-loop vacuum contribution to the mass. At 1-loop in a ϕ^4 theory, this is given by a tadpole graph whose expression can be written as

$$m^2_{1-\text{loop}} = g^2 \int \frac{d^3\boldsymbol{k}}{(2\pi)^3 2k} \left(\frac{1}{2} + f_{\boldsymbol{k}}\right) . \tag{48}$$

Including the vacuum contribution to the mass improves significantly (see the red curve in the figure 4) the agreement between the theoretical prediction and the fit, indicating that higher-order corrections are presumably rather small for this value of the coupling ($g = 1$). Thus, it appears that the quasi-particle description is quite consistent: indeed, the occupation number computed from the fields themselves, when inserted into the 1-loop formula for the effective mass, reproduces very well the mass measured by fitting the peak in the spectral function.

[16] Of course, since the study is performed on a lattice, that has by definition a discrete spectrum, it is impossible to tell whether the distribution has a true $\delta(\boldsymbol{k})$ term at the origin or whether it is a strongly peaked but otherwise regular function.

5.2 Residual interaction energy

A quasi-particle description of a system is useful only if the residual interactions between the quasi-particles are weak – in other words, if the main effect of the interactions is simply to alter the properties of the particles (e.g. by generating an effective mass). This can be tested by computing

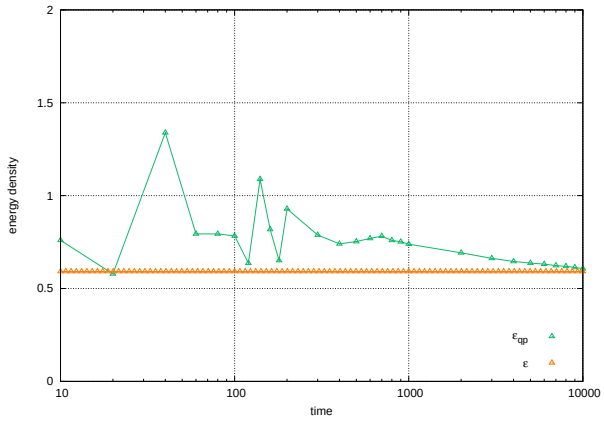

Figure 10: Comparison between the actual energy density of the system (ϵ) and the energy carried by the quasi-particles ($\epsilon_{\rm qp}$) if one neglects their interactions.

the energy density of the system by summing the energies of its quasi-particles, i.e. by assuming that they have no residual interactions[17],

$$\epsilon_{\rm qp} \equiv \int \frac{d^3\boldsymbol{k}}{(2\pi)^3}\, f_{\boldsymbol{k}}\, \sqrt{\boldsymbol{k}^2 + m^2}\,. \tag{49}$$

By comparing this quasi-particle energy to the actual energy density, $\epsilon \equiv \langle T^{00} \rangle$, we can estimate the interaction energy of the quasi-particles and therefore the strength of their residual interactions. The result of this comparison is shown in the figure 10. We see that the true energy of the system is always below the energy of its quasi-particles, indicating that the residual interactions are attractive – which is indeed a standard result of a ϕ^4 field theory. Moreover, as the time increases, the energy of the quasi-particles gets closer to the true energy, meaning that the quasi-particle description is better at late times.

5.3 Entropy production

From the occupation number, it is also possible to compute the entropy density,

$$s \equiv \int \frac{d^3\boldsymbol{k}}{(2\pi)^3} \Big[(1+f_{\boldsymbol{k}}) \ln(1+f_{\boldsymbol{k}}) - f_{\boldsymbol{k}} \ln f_{\boldsymbol{k}} \Big]\,. \tag{50}$$

[17] In our framework, replacing the true energy density by $\epsilon_{\rm qp}$ is equivalent to substituting the expectation value of the interaction energy $\langle V(\varphi) \rangle$ by $\frac{1}{2} m^2 \langle \varphi^2 \rangle$, i.e. to a mean-field approximation.

The time evolution of this quantity is shown in the figure 11 (green curve). One sees that the entropy density is multiplied roughly by a factor 20 during the evolution of the system (the initial value is low in our setup because the occupancy is entirely localized in the zero mode at $t = 0$). In the red curve, we have displayed the entropy that would have a gas of free bosons of equal energy density at thermal equilibrium[18]. The true entropy of the system gets close to the equilibrium entropy, but not exactly equal even at the largest times we have considered (the discrepancy remains of the order of $10 - 20\%$). This difference is presumably a combination of two factors: (i) the fact that the system is not yet fully equilibrated, and (ii) the residual interactions of its quasi-particles.

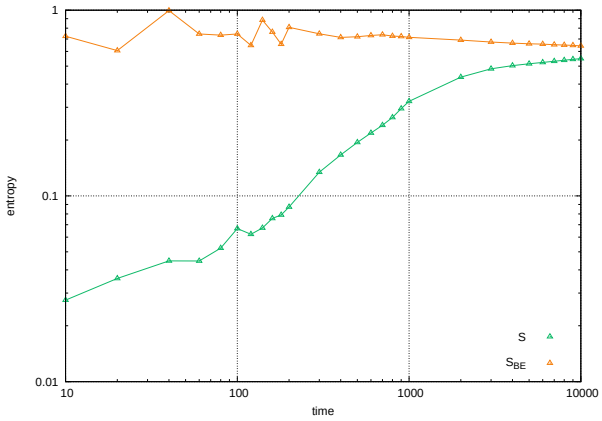

Figure 11: Green curve (S): time evolution of the entropy density s defined in eq. (50). Red curve ($S_{\rm BE}$): entropy of a non-interacting gas of bosons of equal energy density, in thermal equilibrium.

The increase of the entropy defined by eq. (50) may seem paradoxical at first sight, given the way it has been obtained in our framework. Indeed, at the microscopic level, our system is described as an ensemble of classical field configurations that evolve according to the Euler-Lagrange equation of motion. This equation of motion is invariant under time reversal $t \to -t$, yet the entropy s computed in this system is clearly not invariant under this transformation – despite the fact that it is a functional of classical fields that have a time-reversible evolution. Let us recall here that the ensemble of classical field configurations that describe the system in our framework evolves according to the Liouville equation,

$$\partial_t \mathcal{F}_t + \{\mathcal{F}_t, H\} = 0 \, . \tag{51}$$

Instead of eq. (50), one could have defined an entropy based on the probability distribution $\mathcal{F}_t[\varphi, \dot\varphi]$ of the field configurations in phase-space,

$$\mathcal{S} \equiv - \int [D\varphi D\dot\varphi] \; \mathcal{F}_t[\varphi, \dot\varphi] \;\; \ln \mathcal{F}_t[\varphi, \dot\varphi] \; ; \tag{52}$$

and it is easy to see that it is constant in time thanks to Liouville's theorem (see the appendix B). This means that, if one were able to determine the field configuration of the system at a given time,

[18] Its small variations with time are due to the fact that the mass of the quasi-particles is not constant.

there would be no entropy increase because everything would be known about the microscopic state of the system. In contrast, the definition (50) is the appropriate definition when one knows only the single particle distribution in the system. Compared to eq. (52), a lot of information about the microscopic state of the system has been discarded by doing this. This coarse graining is the reason why the entropy given by (50) increases with time, while at the microscopic level the field configurations evolve via time reversible equations.

6 Summary and outlook

In this paper, we have pursued the study started in [48] of the time evolution of a system of scalar fields in a fixed volume box, in a resummation scheme that has been devised to cure the problem of secular divergences caused by parametric resonance. Although it is a resummation of quantum corrections that arise via loops, we have shown that this resummation can also be formulated as an average over classical field trajectories, with a Gaussian ensemble of initial conditions. This latter formulation is the one we adopt for a practical numerical implementation. In [48], we have focused mostly on the evolution of the energy-momentum tensor of the system, and we have shown that the pressure relaxes towards its equilibrium value, thanks to a decoherence mechanism due to the fluctuating initial conditions.

In the present paper, we have studied more microscopic properties of the system, in order to understand in more detail its time evolution. In particular, one question that was left unanswered in [48] is whether the system is in local thermal equilibrium at the time its pressure tensor reaches the equilibrium form. First of all, we have studied the existence of quasi-particles in the spectrum of the theory, by computing the spectral function of the system. Next, after having identified quasi-particle modes, we have computed their occupation number and the associated entropy.

Let us first summarize the main results of this paper in a synthetic way, by displaying in parallel the time evolutions of the various quantities that we have considered separately so far. This is shown in the figure 12. From these plots, it appears that one can divide the time evolution in three stages that are qualitatively distinct[19]:

- **i.** $0 \leq t \leq 100$: at these early times, the pressure of the system has not yet started to relax towards its equilibrium value $p = \epsilon/3$. Moreover, quasi-particles are not a good description of the system (their mass is not well defined, and there are extra spurious branches in the spectral function). The entropy displays only a very moderate growth during this era, the occupation number starts rising in the resonance band almost immediately, but the energy is still almost entirely contained in the zero mode,

- **ii.** $100 \leq t \leq 600$: this intermediate period starts when the occupancy in the resonance band reaches its maximum and starts to subside, while the occupation number rises in the other momentum modes. During this stage, the zero mode still contains the largest share of the total energy, and the remainder is contained predominantly in the resonant modes. The mains features of this era are the relaxation of the pressure towards its equilibrium value, and an important growth of the entropy. In this era, there are well defined quasi-particles, with a mass that is almost constant in time,

[19] The numerical values of the times quoted here are not absolute, but depend on the energy density in the system. Indeed, in a scale invariant theory, all the time-scales vary like $\epsilon^{-1/4}$. Moreover, these time-scales depend on the coupling constant g^2, and decrease as the coupling increases.

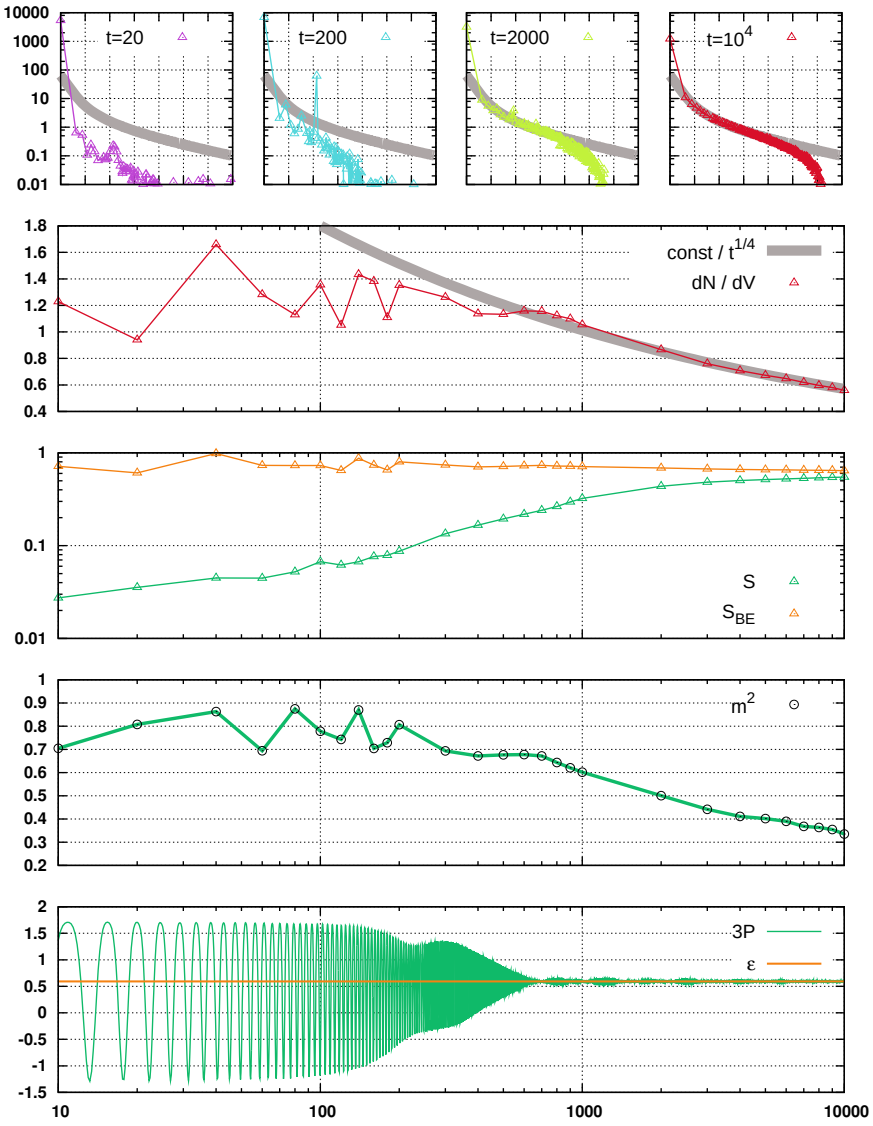

Figure 12: (Panels numbered 1 to 5 from the bottom to the top.) Panel 1: time evolution of the pressure. Panel 2: time evolution of the quasi-particle mass. Panel 3: time evolution of the entropy, compared to the entropy of a gas of same energy density at thermal equilibrium. Panel 4: time evolution of the quasi-particle density. Panel 5: occupation number at various stages of the time evolution (the gray band is a fit at the latest time by a Bose-Einstein distribution with a chemical potential).

iii. $600 \leq t$: in the late stages of the time evolution, the pressure is the equilibrium one, and the entropy displays only a marginal growth. However, the system is not yet fully equilibrated: the mass of the quasi-particles shows a clear decrease, while the occupation number continues to slowly expand towards higher momenta. During this stage, the occupation number shows some signs of Kolmogorov scaling, but perhaps even more compelling is the fact that it seems to evolve as would a system dominated by elastic collisions and which is overpopulated compared to equilibrium – i.e. by developing a chemical potential equal to the mass and a Bose condensate at zero momentum. At the same time, the energy initially contained in the zero mode is progressively distributed among the higher modes.

A very interesting observation is the appearance of a chemical potential, that we interpreted as resulting from a particle excess (compared to the value the particle density should have in equilibrium) combined to a fairly slow rate of inelastic processes. Eventually, the inelastic processes will wipe out the initial particle excess. However, because they are slow, there is an extended regime where the occupation number settles on a form that has a chemical potential. Moreover, for the bosonic statistics, the chemical potential cannot be larger than the mass of the quasi-particles. This implies that if the particle excess is too large, it cannot be accommodated solely by a chemical potential and the system stabilizes itself by the formation of a condensate at zero momentum. Our numerical results confirm this, and moreover indicate that this condensation occurs very early in the time evolution. Interestingly, the condition of overpopulation is also realized for the gluons produced initially in heavy ion collisions. Indeed, at a time Q_s^{-1} (where Q_s is the saturation momentum), the energy density is $\epsilon \sim Q_s^4/g^2$ and the gluon number density is $n \sim Q_s^3/g^2$. Thus one has the dimensionless ratio $n\epsilon^{-3/4} \sim g^{-1/2} \gg 1$, that should be of order 1 in chemical equilibrium. Depending on the strength of the number-changing processes, one may also expect the (transient) appearance of a gluonic chemical potential and the formation of a gluon condensate at zero momentum.

One of the virtues of the formalism we have developed to address this problem is its seamless integration into the color glass condensate framework, since it is formulated in terms of classical field configurations (in fact, the resummation scheme we are using here was obtained as a by-product of the formalism developed for proving the initial state factorization of the large logs of $1/x_{1,2}$). As a consequence, it can be adapted very easily to the Yang-Mills case, and to the study of thermalization in high energy heavy ion collisions. A crucial step in view of this application was performed in [47], where has been derived the spectrum of fluctuations at early times (i.e. before the Glasma instabilities start to develop) for gauge field fluctuations – in a system of coordinates and a gauge that are appropriate for numerical studies of the evolution of the glasma fields.

Let us finally mention some possible connections with the idea of "eigenstate thermalization" proposed by Srednicki in [63] (see also [64, 65, 66]). This idea follows Berry's conjecture [67], which states that the high energy eigenstates of quantum systems whose classical counterpart is chaotic have extremely complicated wave-functions that for all practical purposes can be replaced by a random sum of plane waves (with Gaussian distributed coefficients). Assuming that this conjecture is satisfied, Srednicki proved that sufficiently inclusive measurements on such a state would lead to results that agree with thermal equilibrium. The main impediment to thermalization in a quantum system would thus be the fact that the system is usually not prepared in an energy eigenstate. For instance, for a system that is initially in a coherent state, thermal features would only become manifest once the various energy eigenstates superimposed in the coherent state have become incoherent. In the problem we have considered in the present paper and in [48], the initial

condition at $t = 0$ appears to be closely related to the Wigner distribution of a coherent state and the associated classical dynamics is chaotic. Moreover, we have seen that the relaxation of the pressure is due to the loss of coherence between the various initial conditions. It would thus be very interesting to study whether there is a deeper connection between thermalization in quantum field theory and the ideas advocated by Srednicki.

Acknowledgements

We would like to thank J.P. Blaizot, K. Dusling, K. Fukushima, Y. Hatta, K. Itakura, J. Liao, L. McLerran and R. Venugopalan for useful discussions on the issues studied in this paper and on closely related questions.

A Evolution of the classical phase-space density

In the figure 5, we have obtained a very good fit of the occupation number at late times by a function of the form

$$f_{\boldsymbol{k}} = \frac{T}{\omega_{\boldsymbol{k}} - \mu} - \frac{1}{2} \,. \tag{53}$$

This fit works except for the zero mode, that is over occupied with respect to this distribution. We interpreted this distribution as the classical approximation of a Bose-Einstein distribution, and the $-1/2$ term was simply due to our definition of the occupation number.

However, it is also interesting to forget the underlying quantum field theory we started from, and to consider in its own right the classical problem by which it is approximated. This reformulation is equivalent to solving the Liouville equation,

$$\partial_t \mathcal{F}_t + \{\mathcal{F}_t, \mathcal{H}\} = 0 \,, \tag{54}$$

given some Gaussian initial distribution. Therefore, if we adopt this point of view, we just have a (large) collection of coupled classical oscillators, and we follow their Hamiltonian flow in phase-space. In this appendix, we discuss some aspects of this classical dynamical system, that are relevant to the topics discussed in the rest of the paper.

A.1 Effective Hamiltonian

Motivated by the observation of quasi-particles in the system, we may assume that there is a transformation of the fields and their conjugate momenta such that the Hamiltonian becomes a sum of quasi-free harmonic oscillators coupled only by weak residual interactions. In practice, this amounts to writing

$$\begin{aligned} \mathcal{H} &= \int d^3\boldsymbol{x}\, \frac{1}{2}\Big(\dot\varphi^2 + (\nabla\varphi)^2\Big) + \frac{g^2}{4!}\varphi^4 \\ &= \int d^3\boldsymbol{x}\, \underbrace{\frac{1}{2}\Big(\dot\varphi^2 + (\nabla\varphi)^2 + m^2\varphi^2\Big)}_{\mathcal{H}_0} + \underbrace{\frac{g^2}{4!}\varphi^4 - \frac{1}{2}m^2\varphi^2}_{\mathcal{H}'_{\rm int}} \,. \end{aligned} \tag{55}$$

So far, we have just added and subtracted a mass term by hand, and the parameter m^2 is still arbitrary. In order to make the residual interactions small, one can choose the mean field value for m^2,

$$m^2 = \frac{g^2}{2} \left\langle \varphi^2(x) \right\rangle \ , \tag{56}$$

where the angle brackets denote an ensemble average[20]. The first part of this Hamiltonian can be rewritten as a sum of independent harmonic oscillators by going to Fourier space[21],

$$\mathcal{H}_0 = \int \frac{d^3\boldsymbol{k}}{(2\pi)^3} \underbrace{\frac{1}{2}\left|\dot{\varphi}_{\boldsymbol{k}}\right|^2 + \frac{1}{2}\omega_k^2 \left|\varphi_{\boldsymbol{k}}\right|^2}_{h_{\boldsymbol{k}}} \ , \tag{57}$$

where $\omega_{\boldsymbol{k}} \equiv (\boldsymbol{k}^2 + m^2)^{1/2}$ and where $\varphi_{\boldsymbol{k}}$ is the spatial Fourier transform of φ.

This decomposition of the classical Hamiltonian into elementary harmonic oscillators plus residual interactions is a good starting point to make connections with the study of the occupation number in the previous sections. Indeed, it is easy to check that eq. (44) is equivalent to

$$\frac{1}{2} + f_{\boldsymbol{k}} = \frac{\left\langle h_{\boldsymbol{k}} \right\rangle}{V\omega_{\boldsymbol{k}}} \ . \tag{58}$$

In other words, $\left\langle h_{\boldsymbol{k}} \right\rangle$ is the occupancy of the mode $\boldsymbol{k}$ times $\omega_{\boldsymbol{k}}$ times the volume, plus a constant *vacuum contribution* $V\omega_{\boldsymbol{k}}/2$. This means that one should find a non-zero average value for $\left\langle h_{\boldsymbol{k}} \right\rangle$ even in the vacuum – actual particles in the mode $\boldsymbol{k}$ correspond to an excess of $\left\langle h_{\boldsymbol{k}} \right\rangle$ over $V\omega_{\boldsymbol{k}}/2$.

A.2 Time evolution of the classical distribution

In order to start the discussion, we first plot in the figure 13 the distribution $\mathcal{F}_t[\varphi, \dot{\varphi}]$ of the classical field configurations at various stages of the evolution. Since we obviously cannot plot a functional, we have represented several *Fourier slices*: a slice being defined as the distribution of configurations in the plane[22] $(\sqrt{\omega_{\boldsymbol{k}}/V}|\varphi_{\boldsymbol{k}}|, |\dot{\varphi}_{\boldsymbol{k}}|/\sqrt{\omega_{\boldsymbol{k}} V})$. In the figure 13, we have represented this distribution for three values of $\boldsymbol{k}$: the zero mode, a mode in the resonance band, and a mode at some higher momentum. At the initial time, the zero mode of the fields is highly coherent, and its distribution is concentrated around a single point. In contrast, all the higher modes contain only fluctuations centered around the origin $(0, 0)$, with a width which is that of the vacuum fluctuations (i.e. the width that gives $\left\langle h_{\boldsymbol{k}} \right\rangle = \omega_{\boldsymbol{k}}/2$). At the next time, $t = 200$, the zero mode has decohered and now fills almost uniformly a curve[23] of constant energy. We also see that the distribution of the resonant modes has expanded due to parametric resonance, while the harder modes still have the same distribution as the $t = 0$ one. At later times, the expansion of the resonant modes reaches a

[20] One can check numerically that this mean field expression of the mass is in very good agreement with the measured mass of the quasi-particles.

[21] Note that this and subsequent integrals over $d^3\boldsymbol{k}$ are strongly ultraviolet divergent. In all this appendix, one should have a lattice regularization in mind, so that the number of degrees of freedom in the system is finite.

[22] We rescale the Fourier components in this way so that the vacuum fluctuations look the same for all $\boldsymbol{k}$. A value of $\left\langle h_{\boldsymbol{k}} \right\rangle$ proportional to $\omega_{\boldsymbol{k}}$ corresponds to a circle of fixed radius (of order unity) in this plane.

[23] This is not exactly a curve of constant h_0, as one can see from the fact that it is not a circle. This deviation from a circle is due to the fact that there is a large correction $g^2\varphi_0^4/4!$ coming from the interaction energy. Indeed, the zero mode, because of its large amplitude, is strongly interacting with itself.

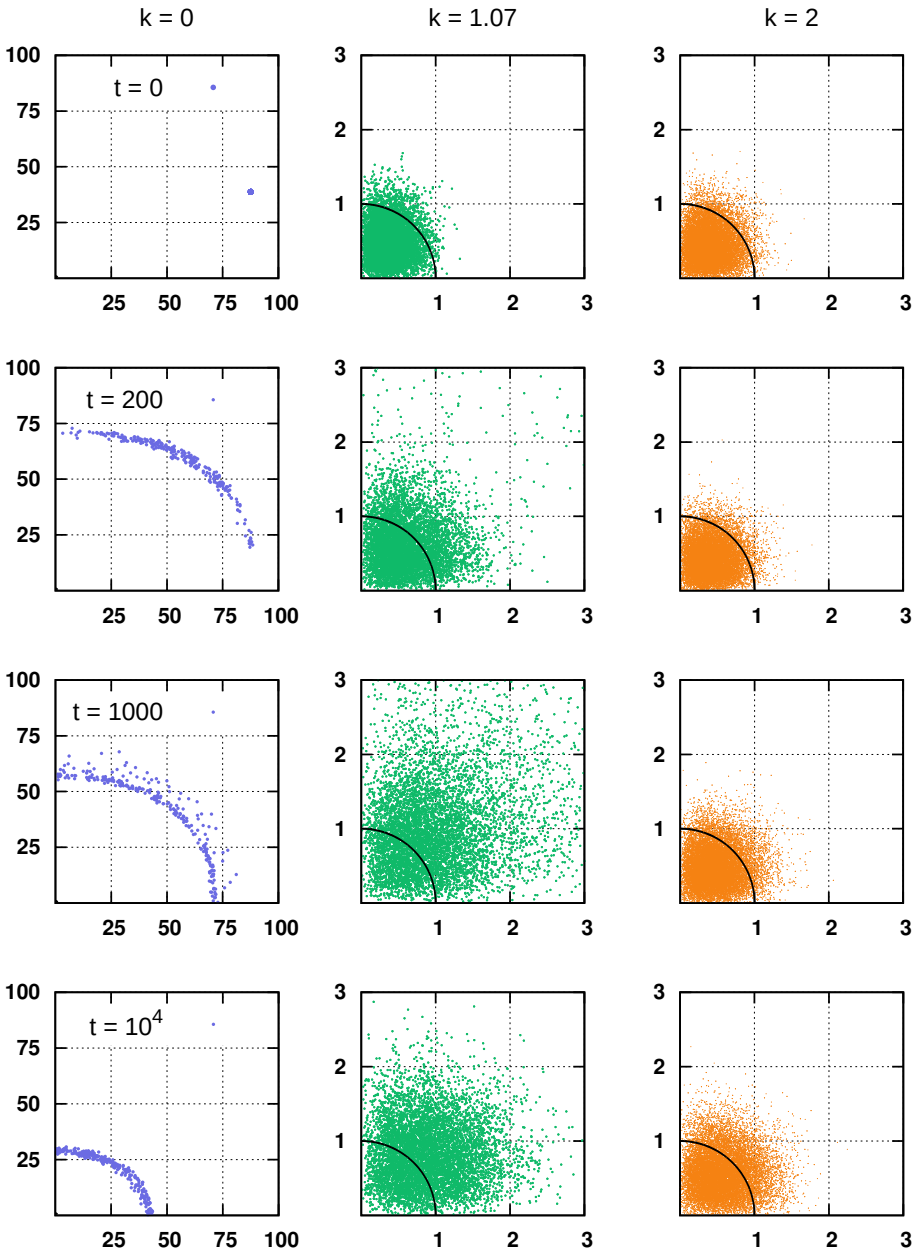

Figure 13: Phase-space density in the $(\sqrt{\omega_{\boldsymbol{k}}/V}|\varphi_{\boldsymbol{k}}|, |\dot{\varphi}_{\boldsymbol{k}}|/\sqrt{\omega_{\boldsymbol{k}}V})$ plane. From left to right: $k = 0$, 1.07 (resonant mode), and 2. From top to bottom: $t = 0$, 200, 10^3 and 10^4. Note the vastly different scale used for the zero mode (left column). The black circle represents the radius of the pure vacuum fluctuations.

maximum and then subsides, while the distribution of the hard modes begins to expand as well. Simultaneously, the zero mode distribution shrinks slowly, while remaining on a curve of constant energy (i.e. this seemingly constant energy is in fact slowly decreasing, due to a transfer of energy from the soft to the hard modes).

To summarize these observations, the Fourier modes that initially have a large amplitude quickly decohere. If there are many such modes (instead of only one as in our numerical example), what happens then depends on whether the classical dynamics is chaotic or on the contrary integrable: in a chaotic system, all these modes mix and fill uniformly an energy shell, while in the integrable case these modes would evolve independently and cover an invariant torus of much smaller dimension (for N modes, an energy shell is a manifold of dimension $2N-1$, while an invariant torus has dimension N only). On larger time scales, the energy carried by these initially large modes decreases slowly, and is transferred to the higher modes whose distribution expands as a consequence of this transfer.

A.3 Asymptotic behavior

What is then the asymptotic distribution $\mathcal{F}_\infty[\varphi,\dot\varphi]$ of these classical fields? Let us assume first that the only quantity that is invariant under the Hamiltonian flow is the energy itself[24]. From the Liouville equation, it is clear that the asymptotic distribution must have a vanishing Poisson bracket with the Hamiltonian. This property is satisfied by any distribution that depends on $\varphi,\dot\varphi$ only through the Hamiltonian $\mathcal{H}[\varphi,\dot\varphi]$. Such an asymptotic form for the distribution $\mathcal{F}_\infty$ has strong implications on the average value of $\langle h_{\boldsymbol{k}}\rangle$. Indeed, if we can neglect the interaction energy (e.g. assuming that most of the interaction energy can be absorbed into an effective mass), then a distribution that depends only on $\mathcal{H}$ implies the equipartition of the energy among the modes,

$$\langle h_{\boldsymbol{k}}\rangle = \text{const (independent of } \boldsymbol{k}) \,. \tag{59}$$

Note that this conclusion holds no matter what is the precise form of the function of $\mathcal{H}$ that $\mathcal{F}_\infty$ is equal to. When equipartition is in the classical phase-space is reached, the occupation number becomes of the form:

$$f_{\boldsymbol{k}} = \frac{\text{const}}{\omega_{\boldsymbol{k}}} - \frac{1}{2} \,. \tag{60}$$

A.4 Asymptotic behavior with constraints

When we try to fit the late time curves of the figure 5 by an expression of the form (60), that lacks the chemical potential μ, the results are not good. This is best seen by plotting $\langle h_{\boldsymbol{k}}\rangle$ (see the figure 14), since eq. (60) would correspond to an horizontal line in this plot. In contrast, the much better fit of the figure 5 could be explained if the average value of $h_{\boldsymbol{k}}$ at late times was of the form

$$\langle h_{\boldsymbol{k}}\rangle = \text{const}\,\frac{\omega_{\boldsymbol{k}}}{\omega_{\boldsymbol{k}}-\mu} \,. \tag{61}$$

This is obvious in the figure 14, where we obtain a good fit to $\left\langle h_{\boldsymbol{k}}\right\rangle$ by an expression of this form.

[24] The total spatial momentum of the system is also conserved, but it does not play any role here because we analyze the problem in the rest frame of the system.

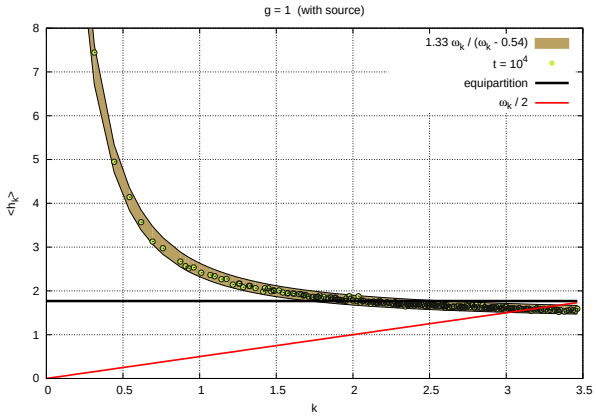

Figure 14: Average value $\langle h_{\boldsymbol{k}} \rangle$ of the energy in the mode $\boldsymbol{k}$. The brown band is a fit of the form $T\omega_{\boldsymbol{k}}/(\omega_{\boldsymbol{k}} - \mu)$, and its width reflects the expected statistical error in our Monte-Carlo simulation. The horizontal line shows the expected result if equipartition is reached. The red line represents the zero point energy $\omega_{\boldsymbol{k}}/2$.

It is possible to understand eq. (61) if one assumes that the Hamiltonian flow not only conserves energy (exactly), but also (to a good degree of approximation) the following quantity[25]

$$\mathcal{N}[\varphi, \dot{\varphi}] \equiv \int \frac{d^3\boldsymbol{k}}{(2\pi)^3} \, \frac{h_{\boldsymbol{k}}}{\omega_{\boldsymbol{k}}} \, . \tag{62}$$

It is obvious that this quantity has a vanishing Poisson bracket with the free quasi-particle part of the Hamiltonian $\mathcal{H}_0$, and that only the residual quasi-particle interactions $\mathcal{H}'_{\rm int}$ can possibly make this quantity change. Thus, if the residual interactions are weak, this quantity should indeed be approximately conserved. If both $\mathcal{H}$ and $\mathcal{N}$ are invariants, then the most general asymptotic solution of the Liouville equation must depend on $\varphi, \dot{\varphi}$ only through some combination of the form $\mathcal{H} - \mu\mathcal{N}$. For any distribution of this form, equipartition is replaced by

$$\left\langle h_{\boldsymbol{k}} - \mu \frac{h_{\boldsymbol{k}}}{\omega_{\boldsymbol{k}}} \right\rangle = \text{const (independent of } \boldsymbol{k}) \, , \tag{63}$$

which leads to eq. (61). Therefore, in the classical dynamical system, the quasi conservation of $\mathcal{N}$ is what explains that we observed an energy distribution that differs considerably from the naive equipartition.

Note that when k is large, eq. (63) is equivalent to $\langle h_{\boldsymbol{k}} \rangle = \text{const}$. This implies that the constant in the right hand side must be positive. Considering now $\boldsymbol{k} = 0$, this imposes $\mu \leq m$. Inserting now eq. (63) in the definition of $\mathcal{N}$,

$$\langle \mathcal{N} \rangle = \int \frac{d^3\boldsymbol{k}}{(2\pi)^3} \, \frac{\text{const}}{\omega_{\boldsymbol{k}} - \mu} \, , \tag{64}$$

[25] The average $\langle \mathcal{N} \rangle$ in the classical dynamical system is the counterpart of the number of quasi-particles in the quantum theory.

we see that it increases with μ, and reaches a finite (because the singularity at $\boldsymbol{k} = 0$ is integrable) maximum when $\mu = m$. However, it may happen that the initial value of $\langle \mathcal{N} \rangle$ is larger than this maximum. In this situation, the $\langle h_{\boldsymbol{k}} \rangle$'s must be altered in order to accommodate this excess, but in such a way that eq. (63) remains valid. Any modification of $\langle h_{\boldsymbol{k}} \rangle$ for $\boldsymbol{k} \neq 0$ will violate eq. (63), so the only possibility is to modify $\langle h_0 \rangle$. Then, we see that the only way to change $\langle h_0 \rangle$ without violating eq. (63) is to have $\mu = m$. Thus, when there is an excess of $\langle \mathcal{N} \rangle$, the equilibrium value of $\langle h_{\boldsymbol{k}} \rangle$ takes the form

$$\langle h_{\boldsymbol{k}} \rangle = A\,\delta(\boldsymbol{k}) + B\,\frac{\omega_{\boldsymbol{k}}}{\omega_{\boldsymbol{k}} - m}\ . \tag{65}$$

This explains why we found a chemical potential whose value is very close to the mass of the quasi-particles (within statistical errors). This phenomenon can be seen as an analogue in classical Hamiltonian dynamics of Bose condensation in quantum mechanics.

A.5 Do vacuum fluctuations thermalize?

The fact that the Liouville evolution makes the distribution $\mathcal{F}_t$ evolve towards a classical thermal equilibrium leads to an interesting question: does the same happen if in our original problem there is no source coupled to the quantum fields, i.e. for pure vacuum fluctuations? In this case, the initial distribution is

$$\mathcal{F}_0[\varphi, \dot{\varphi}] = \exp\left[-\int \frac{d^2\boldsymbol{k}}{(2\pi)^3} \frac{|\dot{\varphi}_{\boldsymbol{k}}|^2 + k^2 |\varphi_{\boldsymbol{k}}|^2}{k} \right], \tag{66}$$

corresponding to $\langle h_{\boldsymbol{k}} \rangle = k/2$. The consistency of our approach requires that the vacuum does not change over time. However, since eq. (66) is not a function of $\mathcal{H}$, our previous considerations suggest that equipartition may also occur if we start from the pure vacuum fluctuations given by eq. (66). We have computed $\langle h_{\boldsymbol{k}} \rangle$ numerically for the pure vacuum case, by starting from the

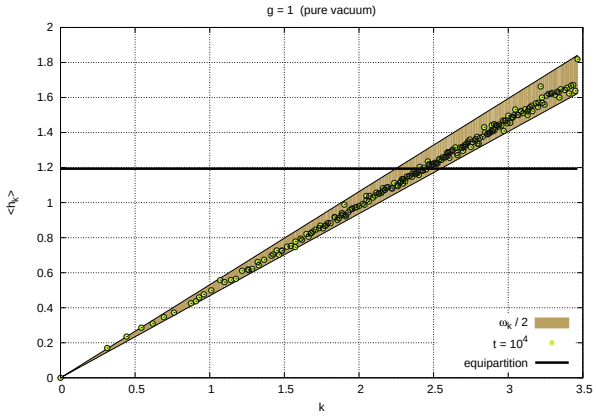

Figure 15: Average value of the energy $h_{\boldsymbol{k}}$ in the mode $\boldsymbol{k}$ for pure vacuum fluctuations. The center of the brown band is $\omega_{\boldsymbol{k}}/2$, and its width reflects the expected statistical error in our Monte-Carlo simulation). The horizontal line corresponds to equipartition.

distribution of eq. (66) and by evolving the corresponding classical field configurations also to a large time $t = 10^4$. As shown in the figure 15, this computation shows no sign of equipartition of the vacuum energy, indicating that the vacuum is stable in our framework.

This is at first sight an intriguing result. Indeed, how does the purely classical Liouville equation know that the distribution of eq. (66) represents the ground state of the corresponding quantum theory? In a sense, the Liouville equation seems to know more than what its "classical" qualifier might suggest. This result can be qualitatively explained by recalling a formal connection that exists between quantum mechanics and the classical Liouville equation. In quantum mechanics, a system can be described by a density operator $\hat{\rho}$, whose evolution is driven by the Von Neumann equation,

$$i\partial_t \hat{\rho} + [\hat{\rho}, H] = 0 \, . \tag{67}$$

It was noted by Wigner and Moyal that this quantum mechanical equation can be formulated equivalently as an evolution in the classical phase-space (see [68] for a recent review). To do this, one should first introduce the Wigner distribution associated to the density operator $\hat{\rho}$. For a single degree of freedom, this is defined as

$$W(q,p) \equiv \int dx \; e^{ipx} \; \big\langle q + x/2 \big| \hat{\rho} \big| q - x/2 \big\rangle \, . \tag{68}$$

The Von Neumann equation can then be shown to be equivalent to the Moyal equation for W,

$$\partial_t W + \{\{W, \mathcal{H}\}\} = 0 \, , \tag{69}$$

where $\{\{\cdot,\cdot\}\}$ is the Moyal bracket, obtained as the Wigner transform of the commutator. At this stage, one has a formulation of quantum mechanics that involves only quantities defined on the classical phase-space (the quantum mechanical aspects are hidden in the fact that the Moyal bracket depends on $\hbar$). The connection to the classical Liouville equation arises via the following two properties,

- **i.** the Moyal bracket $\{\{\cdot, \mathcal{H}\}\}$ is equal to the Poisson bracket $\{\cdot, \mathcal{H}\}$ if the Hamiltonian $\mathcal{H}$ is quadratic in the coordinates and momenta,
- **ii.** for any Hamiltonian, one has

$$\{\{A, B\}\} = \{A, B\} + \mathcal{O}(\hbar^2) \, . \tag{70}$$

If the quantum system is in its ground state $\big|0\big\rangle$, its density operator $\hat{\rho}_0 \equiv \big|0\big\rangle\big\langle 0\big|$ is invariant under the Von Neumann equation. Equivalently, the corresponding Wigner distribution W_0 is invariant under the Moyal equation. Since $\mathcal{F}_0$ is the Wigner distribution of the same vacuum state, it is thus natural that it is left invariant by the Liouville evolution, since it is the $\hbar \to 0$ limit of the invariant Moyal evolution.

B Liouville equation

In this appendix, we recall the derivation of Liouville's equation and some of its well known properties.

B.1 Hamilton's equations

In this appendix, we denote generically the canonical coordinates by $\boldsymbol{Q}$, the corresponding canonical momenta by $\boldsymbol{P}$, and the Hamiltonian by $\mathcal{H}$. Hamilton's equations read

$$\dot{\boldsymbol{Q}} = \frac{\partial \mathcal{H}}{\partial \boldsymbol{P}} \,, \qquad \dot{\boldsymbol{P}} = -\frac{\partial \mathcal{H}}{\partial \boldsymbol{Q}} \,. \tag{71}$$

Let us introduce a few useful notations :

$$\boldsymbol{X} \equiv \begin{pmatrix} \boldsymbol{Q} \\ \boldsymbol{P} \end{pmatrix} \,, \qquad \boldsymbol{\nabla} \equiv \begin{pmatrix} \partial/\partial \boldsymbol{Q} \\ \partial/\partial \boldsymbol{P} \end{pmatrix} \,, \qquad \boldsymbol{V} \equiv \begin{pmatrix} \partial \mathcal{H}/\partial \boldsymbol{P} \\ -\partial \mathcal{H}/\partial \boldsymbol{Q} \end{pmatrix} \,. \tag{72}$$

Hamilton's equations can now be rewritten in the following compact form

$$\dot{\boldsymbol{X}} = \boldsymbol{V} \,. \tag{73}$$

This notation is suggestive of the fact that $\boldsymbol{V}$ is the velocity field induced on phase-space by the Hamiltonian. A crucial property of Hamiltonian flows is that they are incompressible,

$$\boldsymbol{\nabla} \cdot \boldsymbol{V} = 0 \,. \tag{74}$$

This identity is the essence of Liouville's equation.

B.2 Liouville's equation

Consider an ensemble of such dynamical systems, all described by the same Hamiltonian $\mathcal{H}$. At the time t, their distribution in phase-space is described by a density $\mathcal{F}_t[\boldsymbol{Q}, \boldsymbol{P}]$, and we wish to derive an equation that describes the time evolution of this distribution. Naturally, the number of systems in the ensemble is not changing since each system evolves independently of the others. Thus, $\mathcal{F}_t$ is the density for a locally conserved quantity. We have seen before that each point in phase-space moves with the velocity $\boldsymbol{V}$. Therefore, we can write a continuity equation that expresses this conservation,

$$\partial_t \mathcal{F}_t + \boldsymbol{\nabla} \cdot (\mathcal{F}_t \boldsymbol{V}) = 0 \,. \tag{75}$$

By using eq. (74), we can rewrite this equation as[26]

$$\Big[\underbrace{\partial_t + \boldsymbol{V} \cdot \boldsymbol{\nabla}}_{D_t} \Big] \mathcal{F}_t = 0 \,. \tag{76}$$

Note that the term $\boldsymbol{V} \cdot \boldsymbol{\nabla} \mathcal{F}_t$ is nothing but the Poisson bracket $\{\mathcal{F}_t, \mathcal{H}\}$. Thus, we see that both eqs (75) and (76) are equivalent to the usual form of the Liouville equation,

$$\partial_t \mathcal{F}_t + \{\mathcal{F}_t, \mathcal{H}\} = 0 \,. \tag{77}$$

These alternate forms of the Liouville equation are very useful, because they recall us its origin as the continuity equation for the density of systems in phase-space, and because they make some properties of Hamiltonian flows more transparent – in particular thanks to the *flow derivative* D_t introduced in eq. (76).

[26] In the form $D_t \mathcal{F}_t = 0$, the Liouville equation is equivalent to the *Liouville theorem*, that states that $\mathcal{F}_t$ is constant along the Hamiltonian flow lines.

B.3 Basic properties

In this section, we derive some elementary properties of Liouville's equation. To state some of these properties, it will be useful to denote $[d\mathbf{\Gamma}]$ the measure on phase-space.

The most elementary property,

$$\int [d\mathbf{\Gamma}]\, \mathcal{F}_t = \text{const} \,, \tag{78}$$

is in fact just the integral version of Liouville's equation itself. It is simply another way of stating that the number of systems in the ensemble does not change over time. Note that since $\mathcal{F}_t$ is constant along the flow lines, the same is true of any local function $F(\mathcal{F}_t)$. Thus, eq. (78) can be generalized by replacing under the integral $\mathcal{F}_t$ by any function $F(\mathcal{F}_t)$. A similar statement can be made about the energy if we note that[27]

$$D_t \mathcal{H} = 0 \,. \tag{79}$$

(which means that the Hamiltonian does not vary if we follow the flow). Then, by multiplying eq. (76) by $\mathcal{H}$, and by integrating over phase-space, we get

$$\int [d\mathbf{\Gamma}]\, \mathcal{F}_t\, \mathcal{H} = \text{const} \,. \tag{80}$$

This equation simply says that the total energy of our ensemble of systems is conserved.

References

[1] P. Romatschke, U. Romatschke, Phys. Rev. Lett. **99**, 172301 (2007).

[2] M. Asakawa, S.A. Bass, B. Muller, Phys. Rev. Lett. **96**, 252301 (2006).

[3] M. Asakawa, S.A. Bass, B. Muller, Prog. Theor. Phys. **116**, 725 (2007).

[4] L.V. Gribov, E.M. Levin, M.G. Ryskin, Phys. Rept. **100**, 1 (1983).

[5] A.H. Mueller, J-W. Qiu, Nucl. Phys. **B 268**, 427 (1986).

[6] J.P. Blaizot, A.H. Mueller, Nucl. Phys. **B 289**, 847 (1987).

[7] R. Baier, A.H. Mueller, D. Schiff, D. Son, Phys. Lett. **B 502**, 51 (2001).

[8] L.D. McLerran, R. Venugopalan, Phys. Rev. **D 49**, 2233 (1994).

[9] L.D. McLerran, R. Venugopalan, Phys. Rev. **D 49**, 3352 (1994).

[10] L.D. McLerran, R. Venugopalan, Phys. Rev. **D 50**, 2225 (1994).

[11] E. Iancu, A. Leonidov, L.D. McLerran, Lectures given at Cargese Summer School on QCD Perspectives on Hot and Dense Matter, Cargese, France, 6-18 Aug 2001, hep-ph/0202270.

[27] This is due to $\partial_t \mathcal{H} = 0$ and $\boldsymbol{V} \cdot \boldsymbol{\nabla} \mathcal{H} = \{\mathcal{H}, \mathcal{H}\} = 0$.

[12] E. Iancu, R. Venugopalan, Quark Gluon Plasma 3, Eds. R.C. Hwa and X.N. Wang, World Scientific, hep-ph/0303204.

[13] F. Gelis, E. Iancu, J. Jalilian-Marian, R. Venugopalan, Ann. Rev. Part. Nucl. Sci. **60**, 463 (2010).

[14] T. Lappi, Int. J. Mod. Phys. **E20**, 1 (2011).

[15] J. Jalilian-Marian, A. Kovner, L.D. McLerran, H. Weigert, Phys. Rev. **D 55**, 5414 (1997).

[16] J. Jalilian-Marian, A. Kovner, A. Leonidov, H. Weigert, Nucl. Phys. **B 504**, 415 (1997).

[17] J. Jalilian-Marian, A. Kovner, A. Leonidov, H. Weigert, Phys. Rev. **D 59**, 014014 (1999).

[18] J. Jalilian-Marian, A. Kovner, A. Leonidov, H. Weigert, Phys. Rev. **D 59**, 034007 (1999).

[19] J. Jalilian-Marian, A. Kovner, A. Leonidov, H. Weigert, Phys. Rev. **D 59**, 099903 (1999).

[20] E. Iancu, A. Leonidov, L.D. McLerran, Nucl. Phys. **A 692**, 583 (2001).

[21] E. Iancu, A. Leonidov, L.D. McLerran, Phys. Lett. **B 510**, 133 (2001).

[22] E. Ferreiro, E. Iancu, A. Leonidov, L.D. McLerran, Nucl. Phys. **A 703**, 489 (2002).

[23] F. Gelis, T. Lappi, R. Venugopalan, Phys. Rev. **D 78**, 054019 (2008).

[24] F. Gelis, T. Lappi, R. Venugopalan, Phys. Rev. **D 78**, 054020 (2008).

[25] F. Gelis, T. Lappi, R. Venugopalan, Phys. Rev. **D 79**, 094017 (2009).

[26] A. Krasnitz, R. Venugopalan, Phys. Rev. Lett. **86**, 1717 (2001).

[27] A. Krasnitz, R. Venugopalan, Nucl. Phys. **B 557**, 237 (1999).

[28] A. Krasnitz, Y. Nara, R. Venugopalan, Nucl. Phys. **A 727**, 427 (2003).

[29] A. Krasnitz, Y. Nara, R. Venugopalan, Phys. Rev. Lett. **87**, 192302 (2001).

[30] A. Krasnitz, Y. Nara, R. Venugopalan, Nucl. Phys. **A 717**, 268 (2003).

[31] T. Lappi, Phys. Rev. **C 67**, 054903 (2003).

[32] T. Lappi, arXiv:1105.5511 [hep-ph].

[33] A. Krasnitz, R. Venugopalan, Phys. Rev. Lett. **84**, 4309 (2000).

[34] T. Lappi, L.D. McLerran, Nucl. Phys. **A 772**, 200 (2006).

[35] P. Romatschke, R. Venugopalan, Phys. Rev. Lett. **96**, 062302 (2006).

[36] P. Romatschke, R. Venugopalan, Phys. Rev. **D 74**, 045011 (2006).

[37] H. Fujii, K. Itakura, Nucl. Phys. **A 809**, 88 (2008).

[38] H. Fujii, K. Itakura, A. Iwazaki, Nucl. Phys. **A 828**, 178 (2009).

[39] K. Fukushima, F. Gelis, arXiv:1106.1396 [hep-ph].

[40] T.S. Biro, C. Gong, B. Muller, A. Trayanov, Int. J. Mod. Phys. **C 5**, 113 (1994).

[41] U.W. Heinz, C.R. Hu, S. Leupold, S.G. Matinyan, B. Muller, Phys. Rev. **D 55**, 2464 (1997).

[42] T. Kunihiro, B. Muller, A. Ohnishi, A. Schafer, T.T. Takahashi, **A** Yamamoto, Phys. Rev. **D 82**, 114015 (2010).

[43] D.T. Son, hep-ph/9601377.

[44] S.Yu. Khlebnikov, I.I. Tkachev, Phys. Rev. Lett. **77**, 219 (1996).

[45] F. Gelis, T. Lappi, R. Venugopalan, Int. J. Mod. Phys. E **16**, 2595 (2007).

[46] K. Fukushima, F. Gelis, L. McLerran, Nucl. Phys. **A 786**, 107 (2007).

[47] K. Dusling, F. Gelis, R. Venugopalan, arXiv:1106.3927 [nucl-th].

[48] K. Dusling, T. Epelbaum, F. Gelis, R. Venugopalan, Nucl. Phys. **A 850**, 69 (2011).

[49] J. Serreau, hep-ph/0410330.

[50] J. Berges, J. Serreau, Phys. Rev. Lett. **91**, 111601 (2003).

[51] J. Berges, S. Borsányi, J. Serreau, Nucl. Phys. **B 660**, 51 (2003).

[52] G. Aarts, J. Berges, Phys. Rev. Lett. **88**, 041603 (2002).

[53] G. Aarts, J. Berges, Phys. Rev. **D 64**, 105010 (2001).

[54] G. Aarts, N. Laurie, A. Tranberg, Phys. Rev. **D 78** 125028 (2008).

[55] J. Berges, S. Borsanyi, C. Wetterich, Phys. Rev. Lett. **93**, 142002 (2004).

[56] R.D. Pisarski, Phys. Rev. Let. **63**, 1129 (1989).

[57] E. Braaten, R.D. Pisarski, Nucl. Phys. **B 337**, 569 (1990).

[58] J. Kapusta, C. Gale, *Finite temperature field theory; Principles and applications (2nd Edition)*, Cambridge University Press (2006).

[59] P. Arnold, C. Dogan, G.D. Moore, Phys. Rev. **D 74**, 085021 (2006).

[60] A.H. Mueller, D.T. Son, Phys. Lett. **B 582**, 279 (2004).

[61] S. Jeon, Phys. Rev. **C 72**, 014907 (2005).

[62] D. Bernard, cond-mat/0007106, Lectures given at IPhT, Saclay, France (2000).

[63] M. Srednicki, Phys. Rev. E **50**, 888 (1994).

[64] J.M. Deutsch, Phys. Rev. **A 43**, 2046 (1991).

[65] C. Jarzynski, Phys. Rev. E **56**, 2254 (1997).

[66] M. Rigol, V. Dunjko, M. Olshanii, Nature **452**, 854 (2008).

[67] M.V. Berry, J. Phys. A: Math. Gen. **1012**, 2083 (1977).

[68] A. Polkovnikov, Annals Phys. **325**, 1790 (2010).